

# ISVR Technical Memorandum

## SCIENTIFIC PUBLICATIONS BY THE ISVR

**Technical Reports** are published to promote timely dissemination of research results by ISVR personnel. This medium permits more detailed presentation than is usually acceptable for scientific journals. Responsibility for both the content and any opinions expressed rests entirely with the author(s).

**Technical Memoranda** are produced to enable the early or preliminary release of information by ISVR personnel where such release is deemed to be appropriate. Information contained in these memoranda may be incomplete, or form part of a continuing programme; this should be borne in mind when using or quoting from these documents.

**Contract Reports** are produced to record the results of scientific work carried out for sponsors, under contract. The ISVR treats these reports as confidential to sponsors and does not make them available for general circulation. Individual sponsors may, however, authorize subsequent release of the material.

### COPYRIGHT NOTICE

(c) ISVR University of Southampton All rights reserved.

ISVR authorises you to view and download the Materials at this Web site ("Site") only for your personal, non-commercial use. This authorization is not a transfer of title in the Materials and copies of the Materials and is subject to the following restrictions: 1) you must retain, on all copies of the Materials downloaded, all copyright and other proprietary notices contained in the Materials; 2) you may not modify the Materials in any way or reproduce or publicly display, perform, or distribute or otherwise use them for any public or commercial purpose; and 3) you must not transfer the Materials to any other person unless you give them notice of, and they agree to accept, the obligations arising under these terms and conditions of use. You agree to abide by all additional restrictions displayed on the Site as it may be updated from time to time. This Site, including all Materials, is protected by worldwide copyright laws and treaty provisions. You agree to comply with all copyright laws worldwide in your use of this Site and to prevent any unauthorised copying of the Materials.

UNIVERSITY OF SOUTHAMPTON  
INSTITUTE OF SOUND AND VIBRATION RESEARCH  
DYNAMICS GROUP

**Vibration response, sound radiation and sound transmission of an infinite plate strip**

by

**I. Prasetiyo and D.J. Thompson**

ISVR Memorandum No. 994

November 2011

Authorized for issue by  
Professor D.J. Thompson

© Institute of Sound and Vibration Research

## Abstract

The purpose of the work reported here is to understand the vibro-acoustic behaviour of an infinite plate strip in terms of its point mobility, sound radiation and sound transmission loss. Moreover, it aims to provide a benchmark solution for such waveguide structures that can be used by other workers.

Analytical models have been developed for the vibro-acoustic behaviour of the plate strip. The plate strip is assumed to be infinite in length but have a finite width where it is confined by parallel boundaries. Simply supported boundaries are considered for simplicity. The waveguide behaviour allows an analytical wave approach to be considered. This is used to find the free waves in an infinite waveguide, the point mobility, the sound radiation of the structure due to a point force excitation and the sound transmission loss due to acoustic excitation.

From this study, it is shown that the point mobility of the plate strip subject to a point force excitation is stiffness-controlled at low frequency while it tends to be similar to that of an infinite plate at high frequencies. Peaks are found at cut-on frequencies where their magnitudes are dependent on the excitation position. Damping only has an effect around the cut-on frequencies.

The finite width of the plate strip influences the sound power radiation at frequencies below the critical frequency. This leads to the presence of ‘edge modes’, waves with an axial component of wavenumber that is less than that of air. Accordingly, the presence of the edge modes causes the radiated power of the plate strip to be higher than that of the infinite plate in this acoustic short-circuit region. Additionally, the nature of the point force excitation leads to radiation due to the near field in the vicinity of the forcing point.

Compared with an infinite structure, some dips or ripples related to various cut-on frequencies are present in the sound transmission loss curve of the plate strip. Moreover, the slope at low frequencies is modified from the result for an infinite plate when the width is less than half the acoustic wavelength. Apart from this, the sound transmission loss for normal incidence converges to the mass-law result at high frequencies and a stiffness-controlled region appears at frequencies below the first cut-on frequency. For random incidence, the plate strip has a higher transmission loss than the infinite plate below the critical frequency but the results are similar above the critical frequency.

# Contents

Abstract.....	i
Contents .....	ii
Acknowledgements.....	iv
Nomenclature.....	v
1. Introduction .....	1
2. Vibration of a plate strip.....	2
2.1 Undamped free vibration .....	2
2.2 Inclusion of damping .....	6
2.3 Response due to a point force .....	8
2.3.1 Formulation.....	8
2.3.2 Convergence .....	9
2.3.3 Results.....	10
2.3.4 Effect of plate thickness.....	12
2.3.5 Effect of excitation position.....	12
2.3.6 Effect of damping loss factor.....	13
2.3.7 Average response of plate.....	14
2.4 Summary .....	18
3. Sound radiation of a plate strip .....	19
3.1 Infinite plate .....	19
3.2 Plate strip .....	21
3.2.1 Radiation due to point force .....	23
3.2.2 Effect of finiteness and point force excitation on the plate strip .....	25
3.2.3 Effect of damping loss factor.....	30
3.2.4 Effect of plate thickness.....	32
3.2.5 Inclusion of the cross-terms.....	34
3.3 Summary .....	35
4. Sound transmission loss of a plate strip .....	37
4.1 Pressure and velocity functions .....	37
4.2 Transmission coefficient.....	44
4.3 Diffuse sound field.....	52

4.4 Summary .....	53
5. Conclusions .....	55
References .....	56
Appendix A Out-of plane displacement of a plate strip due to a point force .....	58
Appendix B Modulus squared of plate velocity in wavenumber domain .....	61

## **Acknowledgements**

The first author is grateful to Directorate General of Higher Education (DGHE), Department of National Education of Indonesia for providing a postgraduate scholarship.

## Nomenclature

$c$	Sound velocity
$D$	Bending stiffness
$D'$	Complex bending stiffness
$E$	Young's modulus
$f$	Force
$f_y$	$y$ dependent force
$F$	Force amplitude
$F_m$	Fourier coefficients
$h$	Plate thickness
$i = \sqrt{-1}$	Imaginary unit
$k_x, k_y, k_z$	Acoustic wavenumber in $x$ , $y$ and $z$ directions
$k_{x1,m}, k_{x2,m}$	Wavenumber in $x$ -direction for each mode order $m$
$l_y$	Plate strip width
$p$	Acoustic pressure
$p_i$	Incident sound pressure
$p_{rad}$	Radiated pressure
$\tilde{p}$	Fourier transform of $p$
$s$	Stiffness per unit area
$v$	Vibration velocity
$\left\langle v(x, y)^2 \right\rangle_{inf}$	Spatial 'average' mean-square velocity
$\tilde{v}$	Fourier transform of $v$
$w$	Out-of-plane displacement
$w_m$	Complex amplitude of the $m^{\text{th}}$ component
$W_{rad}$	Sound power radiation
$Y$	Structural mobility
$z_a$	Acoustic impedance
$\kappa$	Structural wavenumber in the $x$ -direction

$\nu_p$	Poisson's ratio
$\rho_0$	Fluid density
$\rho$	Plate strip density
$\omega$	Angular frequency
$\omega_m$	$m^{\text{th}}$ cut-on frequency

# 1. Introduction

Complex waveguide structures are often found in practice, for example railway tracks, pipes, bridges, railway carriage floors and many other structures which have a large aspect ratio and constant geometry along the length. It is of importance to understand their dynamic vibro-acoustic behaviour for practical purposes such as noise control. A plate strip is considered here which is assumed to be infinite in length but have a finite width, where it is confined by parallel boundaries. Such structures can also be considered as waveguides [1]. Since such plate strips form a basic element of more complex lightweight structures, they are of importance to be considered first before proceeding to more complex waveguide structures.

The focus of this report is to understand the vibro-acoustic behaviour of a plate strip in terms of its point mobility, sound radiation and sound transmission loss. For this, an analytical model is developed using a wave approach in order to find waves propagating freely along the waveguide. By combining this wave approach with a modal solution in the transverse direction, the response of the plate strip is obtained in the wavenumber domain using the Fourier transform method. This solution is then extended in order to solve more complex cases in which the interaction of the plate strip and the surrounding fluid is considered, i.e. for the case of radiated sound power and sound transmission loss.

The framework for deriving the exact solutions is readily available in some references, e.g. in Ref. [1, 2]. In those references, the structural vibration response and its interaction with surrounding fluid are discussed from a wave phenomenon point of view. This wave approach has been applied to obtain solutions by utilizing a spatial Fourier transform for solving many basic cases e.g. beams, plates, pipes (or cylindrical structures), etc. For the case of a plate strip, some results have also been found for particular cases with a limited discussion.

This report is devoted to a systematic procedure for obtaining solutions for the vibro-acoustic behaviour of the plate strip using the Fourier transform method with emphasis on how they are related to each other. Moreover, a detailed discussion of the implication of varying several parameters of the plate strip is also provided. It is expected that the resulting solutions, which are exact apart from their numerical evaluation, can be used as a benchmark solution for such waveguide structures, for example in validating waveguide finite element/boundary element approaches.

## 2. Vibration of a plate strip

For a waveguide an analytical wave approach can be considered. This is used in this section to find the free waves in an infinite plate strip, and the point mobility. The sound radiation of the structure due to a point force excitation is considered in section 3 and the sound transmission due to acoustic excitation is studied in section 4. Simply supported boundaries on the two parallel edges will be considered throughout for simplicity.

### 2.1 Undamped free vibration

The plate strip under consideration is illustrated in Figure 2.1. It has width  $l_y$  in the  $y$ -direction and is infinite in the  $x$ -direction. It is assumed to be simply supported (pinned) along the edges  $y=0$  and  $y=l_y$ . This condition allows the response to be written in a separable form. A travelling wave solution is used to describe the dependence of the displacement on the  $x$ -direction while, for the  $y$ -direction, a modal solution can be utilized to describe the structural response. Only the out-of-plane response  $w$  is considered here.

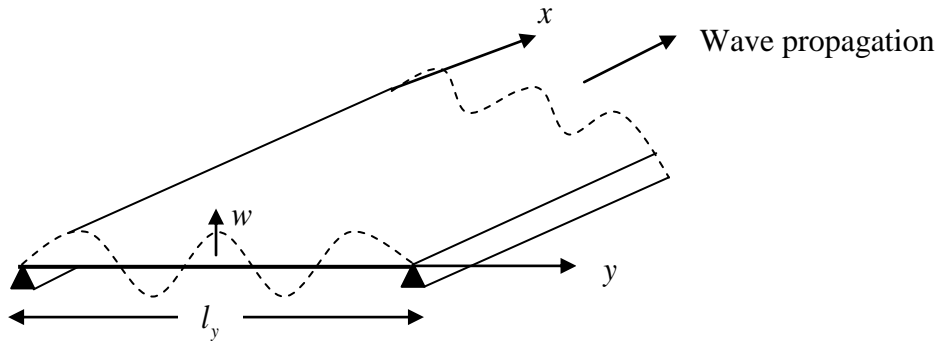


Figure 2.1. A simply-supported plate strip.

For a thin undamped plate, the out-of-plane displacement  $w(x, y, t)$  in the absence of external forces satisfies the following differential equation

$$D \left( \frac{\partial^4 w}{\partial x^4} + 2 \frac{\partial^4 w}{\partial x^2 \partial y^2} + \frac{\partial^4 w}{\partial y^4} \right) + (\rho h) \frac{\partial^2 w}{\partial t^2} = 0 \quad (2.1)$$

where  $D = \frac{Eh^3}{12(1-\nu_p^2)}$  is the bending stiffness,  $E$  is Young's modulus,  $h$  is the plate thickness,  $\nu_p$  is Poisson's ratio, and  $\rho$  is the mass density of the plate.

Harmonic motion is assumed at the angular frequency  $\omega$ , with a time dependence  $e^{i\omega t}$  which is omitted for brevity. Due to the use of simply supported boundaries, the response amplitude  $w$  of the plate at position  $(x, y)$  may be separated into its  $x$  and  $y$  components and written as a summation over components with  $m$  half-sine waves across the width  $l_y$

$$w(x, y) = \sum_{m=1}^{\infty} w_m(x) \sin\left(\frac{m\pi y}{l_y}\right) \quad (2.2)$$

where  $w_m(x)$  is the complex amplitude of the  $m^{\text{th}}$  component that depends on the excitation. This series forms a complete set of functions which satisfy the boundary conditions on  $y=0$  and  $y=l_y$ . Considering one term in the series, substituting this into Eq. (2.1) yields

$$\left( \frac{d^4 w_m}{dx^4} - 2\left(\frac{m\pi}{l_y}\right)^2 \frac{d^2 w_m}{dx^2} + \left(\frac{m\pi}{l_y}\right)^4 w_m \right) - \frac{\rho h}{D} \omega^2 w_m = 0 \quad (2.3)$$

Seeking solutions of the form  $w_m(x) = e^{-ik_{x,m}x}$  gives

$$\left( k_{x,m}^4 + 2\left(\frac{m\pi}{l_y}\right)^2 k_{x,m}^2 + \left(\frac{m\pi}{l_y}\right)^4 \right) - \frac{\rho h}{D} \omega^2 = 0 \quad (2.4)$$

which can be written as

$$\left( k_{x,m}^2 + \left(\frac{m\pi}{l_y}\right)^2 \right)^2 = k_B^4 \quad (2.5)$$

where  $k_B = \sqrt{\omega} \left(\frac{\rho h}{D}\right)^{1/4}$  is the free bending wavenumber of the plate. Eq. (2.5) has four solutions which can be divided into two fundamentally different wave-type solutions for each  $m$

$$\begin{aligned}
k_{x1,m} &= \pm \sqrt{k_B^2 - \left(\frac{m\pi}{l_y}\right)^2} \\
k_{x2,m} &= \pm \sqrt{-k_B^2 - \left(\frac{m\pi}{l_y}\right)^2}
\end{aligned} \tag{2.6}$$

Real wavenumbers represent propagating waves; the wavenumber is the phase change per unit distance, equal to  $2\pi/\lambda$ , where  $\lambda$  is the wavelength of vibration. Imaginary wavenumbers represent evanescent waves which decay with distance. At low frequency,  $k_B < m\pi/l_y$  and all four wavenumbers in Eq. (2.6) are imaginary so that all four waves behave as evanescent or nearfield waves. In contrast, when  $k_B > m\pi/l_y$ ,  $k_{x1,m}$  is real but  $k_{x2,m}$  remains imaginary. Therefore, both propagating waves and nearfield waves are present for the latter case. It may be noted that real positive or negative imaginary values of the wavenumber  $k_{x1,m}$  and  $k_{x2,m}$  correspond to waves travelling or decaying in the positive  $x$ - direction while the opposite sign corresponds to those travelling or decaying in the negative  $x$ - direction. The frequency at which  $k_B = m\pi/l$  is referred to as the  $m^{\text{th}}$  cut-on frequency  $\omega_m$  and is given by

$$\omega_m = \left(\frac{m\pi}{l_y}\right)^2 \left(\frac{D}{\rho h}\right)^{1/2} \tag{2.7}$$

The relation between the wavenumbers  $k_{x1,m}$  and frequency  $\omega$  from Eq. (2.6) can be observed from the dispersion curves shown in Figure 2.2. These are calculated for the example parameters listed in Table 2.1. Clearly, the presence of the boundary constraint has modified the dispersion curves so that  $k_{x1,m} < k_B$ . For each mode  $m$ , as frequency increases, the wavenumbers  $k_{x1,m}$  change from imaginary values into real ones at the cut-on frequencies at which  $k_{x1,m} = 0$ . Conversely, all the wavenumbers  $k_{x2,m}$  are negative imaginary with zero real part. Both  $k_{x1,m}$  and  $k_{x2,m}$  have the same values  $-im\pi/l_y$  at  $\omega = 0$ .

Table 2.1. Material properties and dimension of the plate strip (unless otherwise stated).

Properties	Dimension
Young's modulus, $E$ (N/m <sup>2</sup> )	$7.1 \times 10^{10}$
Poisson's ratio, $\nu_p$	0.332
Thickness, $h$ (mm)	6.0
Width, $l_y$ (m)	1.0
Density, $\rho$ (kg/m <sup>3</sup> )	$2.7 \times 10^3$
Damping loss factor (if used), $\eta$	0.1

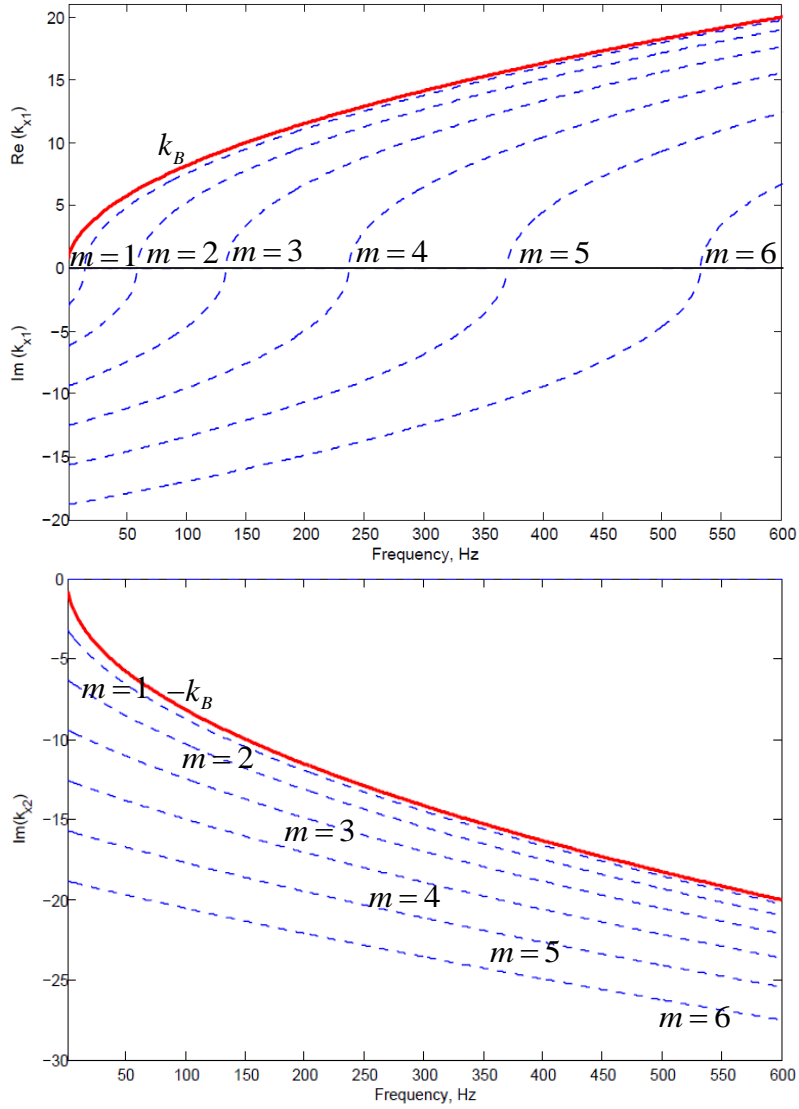


Figure 2.2. The dispersion curves of a simply-supported plate strip (a)  $k_{x1,m}$ ; (b)  $k_{x2,m}$ .

The cut-on frequencies for this plate are listed in Table 2.2. It is noticeable that they are proportional to  $m^2$  as indicated in Eq. (2.7).

Table 2.2. Cut-on frequencies for each mode  $m$  in Hz.

$m$	$f_m$
1	14.8
2	59.2
3	133
4	237
5	370
6	533
7	725
8	947
9	1198
10	1479
11	1790
12	2130
13	2500
14	2899
15	3328

## 2.2 Inclusion of damping

Up to this point, the equations have been derived for an undamped structure. In practice, however, all structures experience damping. In order to incorporate this, a damping loss factor  $\eta$  is included in the formulation by making the Young's modulus complex. The bending stiffness becomes

$$D' = \frac{E(1+i\eta)h^3}{12(1-\nu_p^2)} \quad (2.8)$$

From now on, this complex bending stiffness  $D'$  will be used.

Due to the introduction of the complex bending stiffness, the wavenumbers in Eq. (2.6) become complex. Therefore, there are no purely propagating waves or purely evanescent waves in this case as both of them are decaying oscillatory waves. Moreover, since Eq. (2.6) produces wavenumber values in which the imaginary part

can be either positive or negative, in the calculation process it must be ensured that the complex wavenumbers have imaginary values less than zero for positive-going waves in order to obtain waves that decay as  $x \rightarrow \infty$ .

Figure 2.3 shows examples of complex wavenumbers for  $\eta = 0.1$  and the same parameters as previously, see Table 2.1. Results are shown for  $m=1$  to  $m=6$ . The wavenumbers  $k_{x1,m}$  can be seen to be predominantly imaginary at low frequency and then to become predominantly real above the cut-on frequency. However, this transition is more gradual than for the undamped case. The wavenumbers  $k_{x2,m}$  are negative imaginary wavenumbers with a small negative real part.

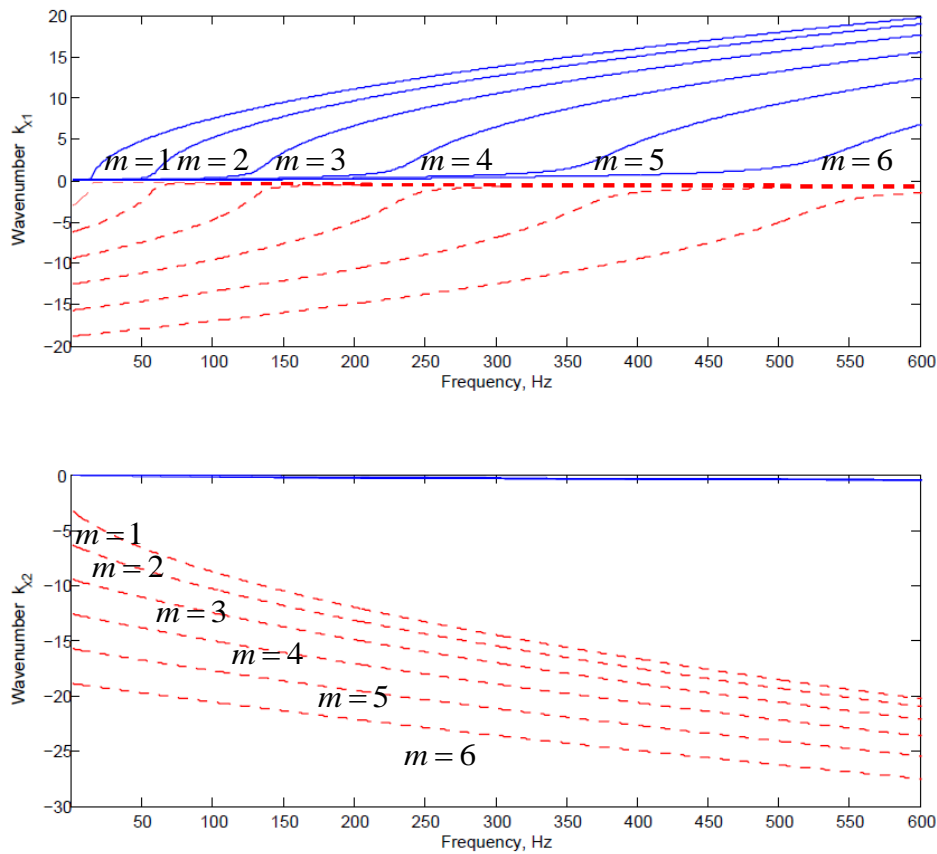


Figure 2.3. Complex wavenumber evolution against frequency (— real components; --- imaginary components).

## 2.3 Response due to a point force

### 2.3.1 Formulation

There are four wave solutions for each  $m$  in Eq. (2.6), allowing the complete solution to be written as

$$w(x, y) = \sum_m \left\{ A_{1,m} e^{ik_{x1,m}x} + A_{2,m} e^{ik_{x2,m}x} + A_{3,m} e^{-ik_{x1,m}x} + A_{4,m} e^{-ik_{x2,m}x} \right\} \sin\left(\frac{m\pi y}{l_y}\right) \quad (2.9)$$

In order to determine the constants  $A_{1,m}$ ,  $A_{2,m}$ ,  $A_{3,m}$  and  $A_{4,m}$ , boundary conditions are required. For a force applied at  $x=0$  it should be noted that, to ensure that waves decay in both directions,  $A_{1,m}$  and  $A_{2,m}$  are zero in the region  $x \geq 0$  while  $A_{3,m}$  and  $A_{4,m}$  are zero in the region  $x \leq 0$ . The external force can be written as a pressure  $f(x, y)$

$$f(x, y) = f_x(x)f_y(y) \quad (2.10)$$

where  $f_x(x) = \delta(x-0)$  and  $f_y(y) = F\delta(y-y_0)$  for a point force at  $(0, y_0)$ . Since the Fourier transform of  $f_x(x) = \delta(x-0)$  into the wavenumber domain is unity at all wavenumbers, it is sufficient to consider only  $f_y(y)$ . Due to the finite width of the plate and the simply supported boundary conditions, this can be expressed as a Fourier sine series as follows

$$f_y(y) = \sum_{m=1}^{\infty} F_m \sin\left(\frac{m\pi}{l_y} y\right) \quad (2.11)$$

where  $F_m$  are the Fourier coefficients which are given by

$$F_m = \frac{2}{l_y} \int_0^{l_y} f_y(y) \sin\left(\frac{m\pi}{l_y} y\right) dy \quad (2.12)$$

Recalling  $f_y(y) = F\delta(y-y_0)$ , Eq. (2.12) becomes

$$F_m = \frac{2F}{l_y} \sin\left(\frac{m\pi}{l_y} y_0\right) \quad (2.13)$$

where  $F$  is the force amplitude.

Considering the continuity of displacement, rotation and bending moment and the force equilibrium condition at  $x=0$ , the solution may be written as follows (see Appendix A for its detailed derivation)

$$\begin{aligned} w(x \leq 0, y) &= \sum_{m=1}^{\infty} \frac{-iF_m}{2D'k_{x1,m}(k_{x1,m}^2 - k_{x2,m}^2)} \left[ e^{ik_{x1,m}x} - \frac{k_{x1,m}}{k_{x2,m}} e^{ik_{x2,m}x} \right] \sin\left(\frac{m\pi y}{l_y}\right) \\ w(x \geq 0, y) &= \sum_{m=1}^{\infty} \frac{-iF_m}{2D'k_{x1,m}(k_{x1,m}^2 - k_{x2,m}^2)} \left[ e^{-ik_{x1,m}x} - \frac{k_{x1,m}}{k_{x2,m}} e^{-ik_{x2,m}x} \right] \sin\left(\frac{m\pi y}{l_y}\right) \end{aligned} \quad (2.14)$$

From this, the mobility  $Y = i\omega w/F = \dot{w}/F$  for the infinite plate strip can be derived as

$$\frac{\dot{w}(x, y)}{F} = i\omega \sum_{m=1}^{\infty} \frac{-i(2/l_y) \sin(m\pi y_0/l_y)}{2D'k_{x1,m}(k_{x1,m}^2 - k_{x2,m}^2)} \left[ e^{-ik_{x1,m}|x|} - \frac{k_{x1,m}}{k_{x2,m}} e^{-ik_{x2,m}|x|} \right] \sin\left(\frac{m\pi y}{l_y}\right) \quad (2.15)$$

The point mobility for the structure can be found by setting  $x=0$  and  $y=y_0$

$$Y(\omega) = \sum_{m=1}^{\infty} \frac{\omega}{D'l_y k_{x1,m}(k_{x1,m}^2 - k_{x2,m}^2)} \left[ 1 - \frac{k_{x1,m}}{k_{x2,m}} \right] \sin^2\left(\frac{m\pi}{l_y} y_0\right) \quad (2.16)$$

Note that as an alternative formulation it is possible to apply the residue calculus method to obtain the point mobility  $Y$  [2].

### 2.3.2 Convergence

Theoretically, the response amplitude of the plate strip is obtained from an infinite number of the wave components. In practice, the summation in Eq. (2.2), (2.9), (2.14) and (2.16) is performed for  $m=1$  to  $M$ , where the upper limit  $M$  is determined based on some convergence criterion. In order to find a suitable criterion, the mobility was calculated at various representative frequencies (30 Hz, 200 Hz, 400 Hz, 1 kHz, 2 kHz, and 3 kHz) for different values of  $M$  with excitation at the position  $(0, 0.433l_y)$ . From Table 2.2, it can be seen that at 30 Hz a single wave has

cut on, at 200 Hz 3 waves, at 400 Hz 5 waves, at 1 kHz 8 waves, at 2 kHz 11 waves and at 3 kHz 14 waves. Results are shown in Figure 2.4 in terms of a relative difference in  $|Y|$  compared with  $M = 400$ . From this, it can be concluded that  $M = 81$  will give results within 1% for 3 kHz which is the highest frequency considered. The required upper limit  $M$  decreases for lower frequencies but the ratio of this to the number of waves that have cut-on at each of these frequencies tends to be constant. From this convergence study, a ratio of 6 (i.e.  $M$  is taken as 6 times the number of cut-on modes) is found to be sufficient to estimate the mobility within 1% for a particular frequency of interest.

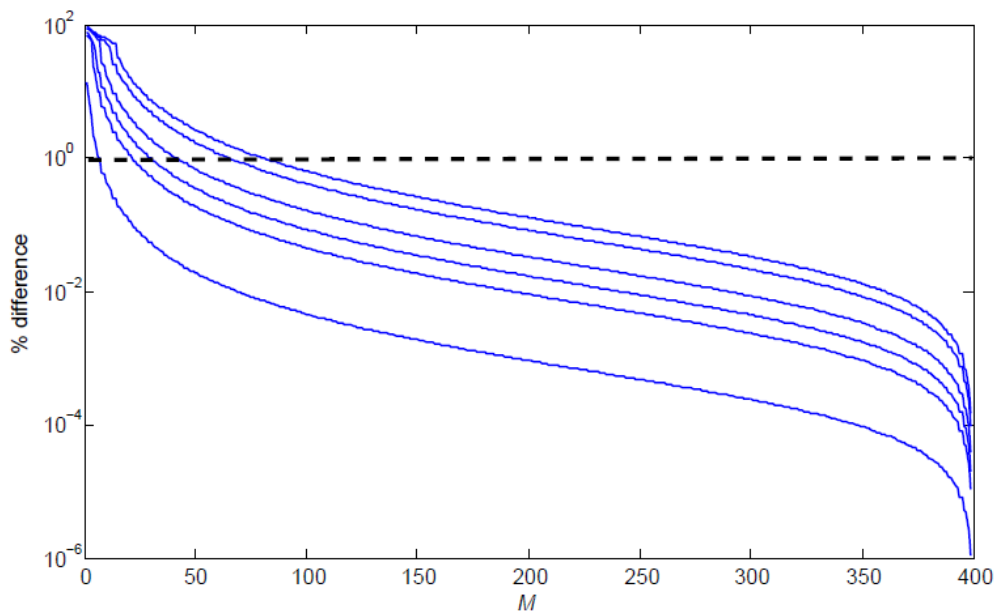


Figure 2.4. Percentage difference relative to  $M = 400$  for different values of  $M$ . From lower to upper curve the results correspond to 30 Hz, 200 Hz, 400 Hz, 1 kHz, 2 kHz, and 3 kHz. The dashed line indicates 1% difference.

### 2.3.3 Results

Figure 2.5 shows the point mobility of a plate strip with properties as in Table 2.1 for excitation at position  $(0, 0.433l_y)$ . The mobility of an infinite plate with the same properties is shown for comparison. This is given by  $Y = 1/8\sqrt{D'(\rho h)}$  [3].

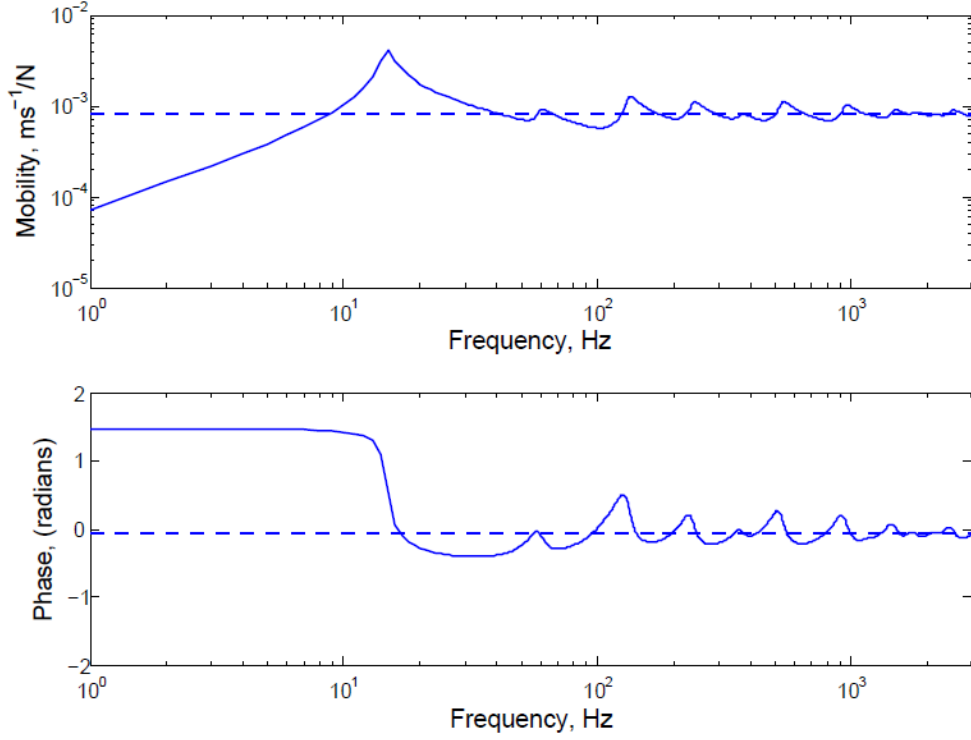


Figure 2.5. The point mobility of the plate strip excited at position  $(0, 0.433l_y)$ . The dashed line indicates the mobility of an infinite plate.

The features of the plate strip mobility in Figure 2.5 can be identified as follows

1. At low frequencies, below the first cut-on frequency, the mobility is clearly stiffness-controlled as indicated by the phase of nearly  $\pi/2$  radians and the amplitude which increases in proportion to frequency. Note that the phase is less than  $\pi/2$  radians due to the presence of the damping loss factor which makes the stiffness complex. It is also seen from the point mobility formula where  $k_B \ll (m\pi/l_y)$  at this frequency region hence Eq. (2.16) reduces to

$$Y(\omega) = i \sum_{m=1}^{\infty} \frac{\omega}{2D'm\pi} \left( \frac{\sin(m\pi y_0/l_y)}{m\pi/l_y} \right)^2 \quad (2.17)$$

2. Peaks occur at each of the cut-on frequencies (see Table 2.2).
3. At high frequencies, when a lot of waves have cut on, the mobility tends to be similar to that of an infinite plate.

### 2.3.4 Effect of plate thickness

It is instructive to study the point mobility behaviour due to changes in the plate thickness. Three different plate thicknesses are considered, 3 mm, 6 mm and 9 mm. The results are shown in Figure 2.6. It is clear that reducing the plate thickness leads to a higher mobility and a reduction in the cut-on frequencies.

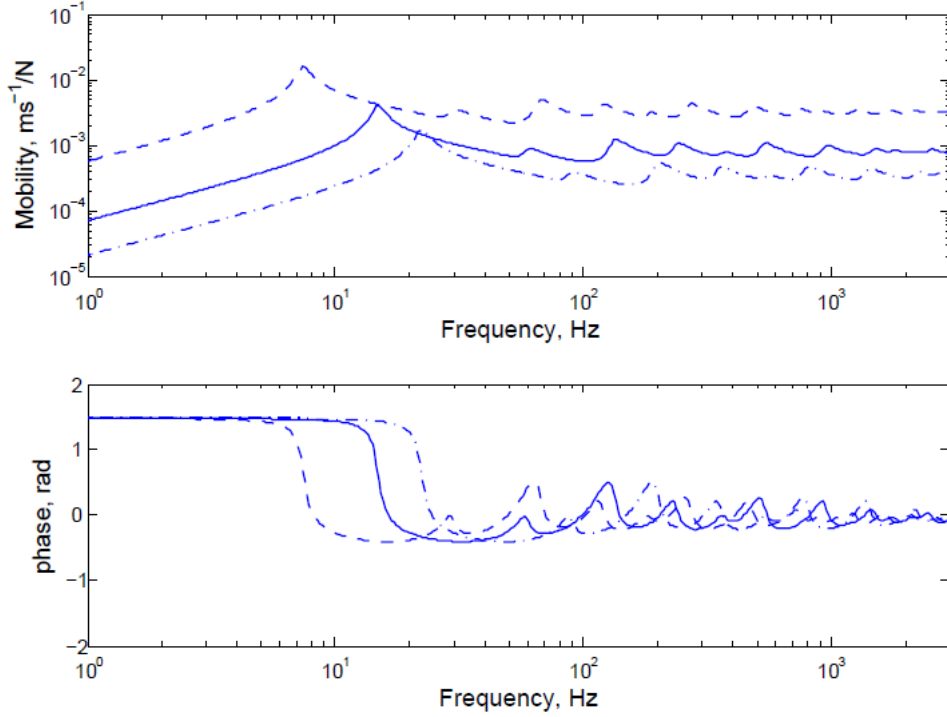


Figure 2.6. Effect of plate thickness on the point mobility excited at  $(0, 0.433l_y)$

(---  $h = 3$  mm; —  $h = 6$  mm; · - ·  $h = 9$  mm).

### 2.3.5 Effect of excitation position

The peaks at the cut-on frequencies have magnitudes that are determined by the term  $\sin^2(m\pi y_0/l_y)$  in Eq. (2.16). Figure 2.7 shows the point mobility for  $y_0 = l_y/4$  and  $y_0 = l_y/2$ . For the case of excitation at the centre position ( $y_0 = l_y/2$ ), the peaks only exist when  $m = 1, 3, 5, \dots$  etc, as the even ones are missing since  $\sin(m\pi y_0/l_y) = 0$ . Meanwhile, for the case of  $y_0 = l_y/4$  the peaks are found for  $m = 1, 2, 3, 5, 6, 7$  etc while those for  $m = 4, 8, \dots$  etc are missing. Again, the term  $\sin(m\pi y_0/l_y) = 0$  for these values of  $m$ . For the latter case, the low frequency

stiffness-like behaviour corresponds to a higher stiffness (lower mobility) because this position is closer to the edge.

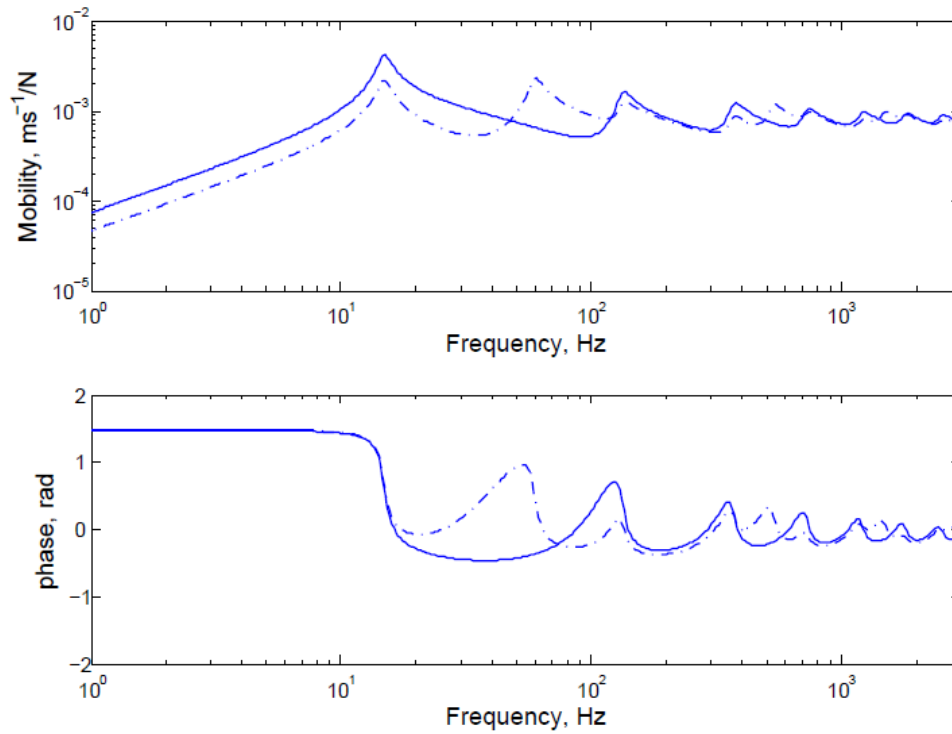


Figure 2.7. Modulus and phase of point mobility for an infinite plate strip (— at  $(0, l_y/2)$ ; - - - at  $(0, l_y/4)$ ).

### 2.3.6 Effect of damping loss factor

To show the effect of the damping loss factor on the mobility, Figure 2.8 compares results with  $\eta = 0.01$  and  $\eta = 0.1$  for excitation at the centre position. This figure shows that a lower damping loss factor causes a higher amplitude at the peaks, whereas a higher damping suppresses the peak amplitude. Away from the peaks, the response is similar. So, it is clear that the greatest damping effect on the point mobility can be seen in the region of the peaks which correspond to the cut-on frequencies.

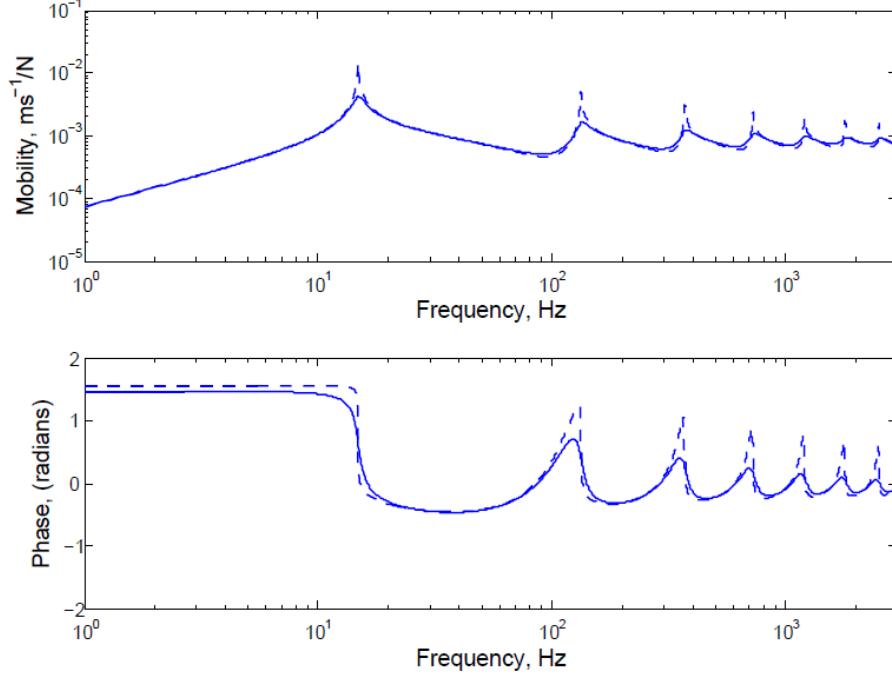


Figure 2.8. Effect of damping loss factor on the point mobility (---  $\eta = 0.01$ ; —  $\eta = 0.1$ ).

### 2.3.7 Average response of plate

In this section the spatial average response of the plate is determined. The vibration of the plate surface in Eq. (2.15) can be expressed as a two dimensional Fourier transforms as follows

$$v(x, y) = \frac{1}{4\pi^2} \int_{-\infty}^{\infty} \int_{-\infty}^{\infty} \tilde{V}(k_x, k_y) e^{-i(k_x x + k_y y)} dk_x dk_y \quad (2.18)$$

The wavenumber transform of  $v(x, y)$  for a single mode  $m$  is

$$\begin{aligned} \tilde{V}(k_x, k_y) = & \frac{\omega F_m}{2D'k_{x1,m}(k_{x1,m}^2 - k_{x2,m}^2)} \left[ \int_{-\infty}^0 \left( e^{i(k_{x1,m} + k_x)x} - \frac{k_{x1,m}}{k_{x2,m}} e^{i(k_{x2,m} + k_x)x} \right) dx \right. \\ & \left. + \left( \int_0^{\infty} e^{-i(k_{x1,m} - k_x)x} - \frac{k_{x1,m}}{k_{x2,m}} e^{-i(k_{x2,m} - k_x)x} \right) dx \right] \left[ \int_0^{l_y} \left( \frac{e^{i(m\pi/l_y + k_y)y} - e^{-i(m\pi/l_y - k_y)y}}{2i} \right) dy \right] \end{aligned} \quad (2.19)$$

where the integration limit  $\pm\infty$  in the  $y$ -direction is replaced by 0 to  $l_y$  because it is assumed that the velocity is zero outside this range (for a plate set in a baffle). Eq.(2.19) has the following solution

$$\tilde{V}(k_x, k_y) = \frac{i\omega F_m}{D'(k_{x1,m}^2 - k_x^2)(k_{x2,m}^2 - k_x^2)} \frac{(m\pi/l_y)[(-1)^m e^{ik_y l_y} - 1]}{[k_y^2 - (m\pi/l_y)^2]} \quad (2.20)$$

The mean-square response at a given point is the integration of the squared velocity over time. For harmonic motion with complex velocity amplitude  $v(x, y)$ , this is equal to  $|v(x, y)|^2/2$ . It can also be written in terms of the product of the complex velocity amplitude  $v(x, y)$  and its conjugate  $v^*(x, y)$ . A spatial ‘average’ mean-square response can then be obtained by integrating  $\overline{v(x, y)^2}$  over the plate strip area

$$\left\langle \overline{v(x, y)^2} \right\rangle_{\text{inf}} = \frac{1}{l_y} \int_0^{l_y} \int_{-\infty}^{\infty} \overline{v(x, y)^2} dx dy \quad (2.21)$$

where  $\langle \dots \rangle_{\text{inf}}$  denotes a spatial ‘average’ over the width. Note that this is actually an integral over the length direction rather than an average due to the infinite extent of the plate strip. For convenience, an index *inf* is added to the angle brackets to indicate this. Recalling the definition of the mean-square response and substituting Eq. (2.18) into Eq. (2.21), this yields

$$\begin{aligned} \left\langle \overline{v(x, y)^2} \right\rangle_{\text{inf}} = & \sum_{m=1}^{\infty} \sum_{m'=1}^{\infty} \frac{1}{l_y} \frac{1}{32\pi^4} \int_{-\infty}^{\infty} \int_{-\infty}^{\infty} \text{Re} \left\{ \left[ \int_{-\infty}^{\infty} \int_{-\infty}^{\infty} \tilde{V}(k_x, k_y) e^{-i(k_x x + k_y y)} dk_x dk_y \right. \right. \\ & \left. \left. \times \int_{-\infty}^{\infty} \int_{-\infty}^{\infty} \tilde{V}^*(k'_x, k'_y) e^{i(k'_x x + k'_y y)} dk'_x dk'_y \right] \right\} dx dy \end{aligned} \quad (2.22)$$

where  $k'_x$  and  $k'_y$  are introduced to distinguish between the integration over  $k_x$  and  $k_y$  related to  $\tilde{V}$  and  $\tilde{V}^*$  respectively. If the integration order is changed so that integration is first performed over  $x$  and  $y$ , use can be made of the Dirac delta function as follows

$$\int_{-\infty}^{\infty} \int_{-\infty}^{\infty} e^{i(k'_x - k_x)x} e^{i(k'_y - k_y)y} dx dy = 4\pi^2 \delta(k'_x - k_x) \delta(k'_y - k_y) \quad (2.23)$$

where the integral is zero for  $k_x \neq k'_x$  or  $k_y \neq k'_y$  and is infinite if  $k_x = k'_x$  and  $k_y = k'_y$ .

Thus, the average mean-square response can be obtained in terms of the surface velocity in the wavenumber domain as follows

$$\left\langle \overline{v(x, y)^2} \right\rangle_{\text{inf}} = \sum_{m=1}^{\infty} \frac{1}{l_y} \frac{1}{8\pi^2} \int_{-\infty}^{\infty} \int_{-\infty}^{\infty} |\tilde{V}(k_x, k_y)|_m^2 dk_x dk_y \quad (2.24)$$

where  $|\tilde{V}(k_x, k_y)|_m^2$  is defined as

$$|\tilde{V}(k_x, k_y)|_m^2 = \left| \frac{\omega F_m}{D'(k_{x1,m}^2 - k_x^2)(k_{x2,m}^2 - k_x^2)} \right|^2 \left[ \frac{2\pi m / l_y}{k_y^2 - (m\pi/l_y)^2} \right]^2 \sin^2 \left( \frac{k_y l_y - m\pi}{2} \right) \quad (2.25)$$

which reflects the energy spectrum of  $\tilde{V}(k_x, k_y)$ . The derivation of Eq. (2.25) is given in Appendix B. In determining the squared-amplitude of the surface velocity for each mode order in Eq. (2.25) the cross-term contributions have been neglected.

Figure 2.9 presents the average response of the plate strip with different damping loss factors. It is clear that the damping loss factor has a significant impact above the first cut-on frequency with the largest influence found around the cut-on frequencies. In this frequency region, away from the cut-on frequencies, it can be seen that the average response is inversely proportional to the damping loss factor. Hence, increasing of the damping loss factor gives reduction of the average response. Below the cut-on frequency, the response is largely unaffected by the damping.

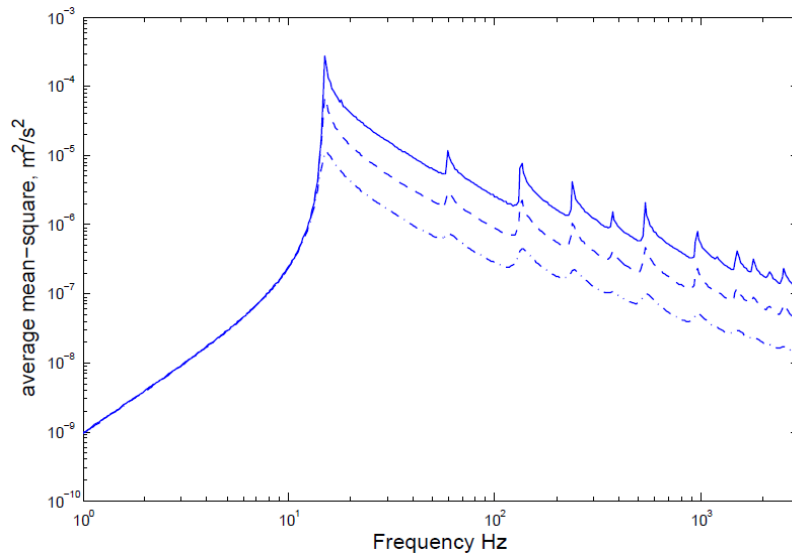


Figure 2.9. Average response of the plate strip with different damping loss factor  $\eta$  (—  $\eta = 0.01$ ; ---  $\eta = 0.03$ ; · - · - ·  $\eta = 0.1$ )

The effect of thickness on the average response can be observed from Figure 2.10. In general, the thinner plate has lower average response compared with a thicker one. The peak associated with the first cut-on frequency shifts to a lower frequency as the thickness of the plate strip is reduced. The implication of these results will be discussed further in section 3 where the radiation ratio, which is the sound radiation normalized to the average response of the plate, is investigated.

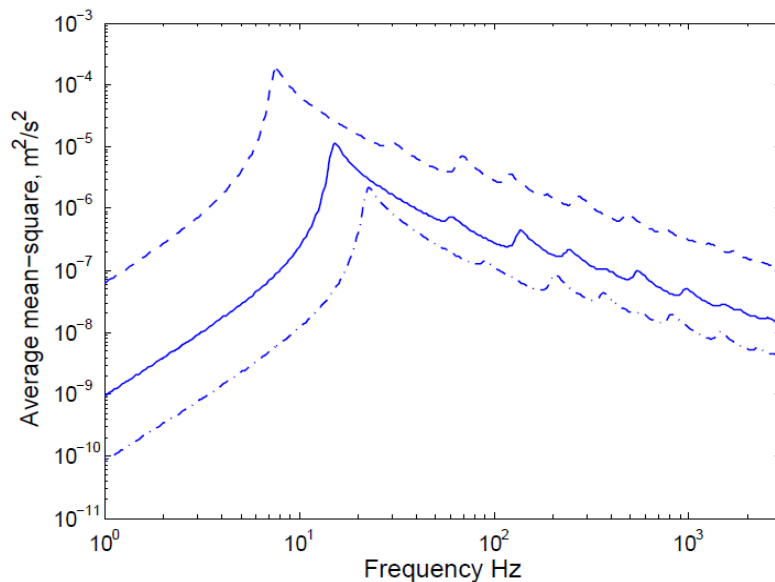


Figure 2.10. Average response of the plate strip due to different thickness with damping loss factor equal to 0.1 and excited at  $(0, 0.433l_y)$  (---  $h = 3$  mm; —  $h = 6$  mm; - · - ·  $h = 9$  mm).

## 2.4 Summary

The point mobility behaviour of the plate strip is stiffness-controlled at low frequency and then tends to the mobility of an infinite plate at high frequencies. Peaks are found in the mobility curve associated with the cut-on frequencies while their magnitude is determined by the term  $\sin^2(m\pi y_0/l_y)$ . The damping has a significant effect at the cut-on frequencies while in other areas there is little effect on the point mobility. However the spatially averaged response is affected by the damping at all frequencies above the first cut-on frequency. Moreover, the average response is also affected by the thickness of the plate strip.

To get an acceptable accuracy, a sufficient number of waves should be incorporated in the calculation, indicated by the upper limit  $M$ . It has been shown that the ratio of  $M$  to the number of waves that have cut-on should be at least 6 to obtain the response within 1%.

### 3. Sound radiation of a plate strip

A vibrating plate in contact with a fluid will radiate sound by producing acoustic waves that propagate away from the plate surface. In this section, the sound radiation from the plate strip is evaluated by means of an analytical model. The analytical model uses a wave-domain approach in two dimensions.

In order to understand the sound radiation mechanism for an infinite plate strip, a two-dimensional spatial (or wavenumber) Fourier transform is used for predicting the sound radiated in the wavenumber domain. In this evaluation, a wave approach as above is used to determine the velocity distribution of the plate strip in the infinite direction. The basic concept of using the wavenumber domain approach for the sound radiation is introduced through an infinite plate case. It is then extended to the plate strip case by imposing simply supported boundaries on the two parallel edges while assuming that the plate strip is set in an infinite rigid baffle. A detailed explanation of the radiated power calculation in the wavenumber domain can be found in [1, 4, 5].

#### 3.1 Infinite plate

Consider first an infinite, uniform plate which is in contact with a semi-infinite fluid domain  $z > 0$ , as shown in Figure 3.1. A plane transverse wave is assumed to travel in the plate in the  $x$ -direction with arbitrary frequency  $\omega$  and wavenumber  $\kappa$ . The velocity amplitude with the implicit time dependence  $e^{i\omega t}$  is expressed by

$$v(x) = V e^{-i\kappa x} \quad (3.1)$$

Subsequently, sound is radiated by the vibrating plate into the fluid with the same wavenumber component in the  $x$ -direction.

In terms of the acoustic field, a plane wave propagates with a component in the  $x$ -direction and a component in the  $z$ -direction

$$p(x, z) = P e^{-i(k_x x + k_z z)} \quad (3.2)$$

The acoustic plane waves must have a wavenumber component in the  $x$ -direction equal to that of the wave in the plate  $k_x = \kappa$ . This leads to the wavenumber in the  $z$ -direction being given by

$$k_z = \pm(k^2 - \kappa^2)^{1/2} \quad (3.3)$$

where  $k = \omega/c$  is the acoustic wavenumber in the fluid at frequency  $\omega$  and  $c$  is the wave speed in the fluid.

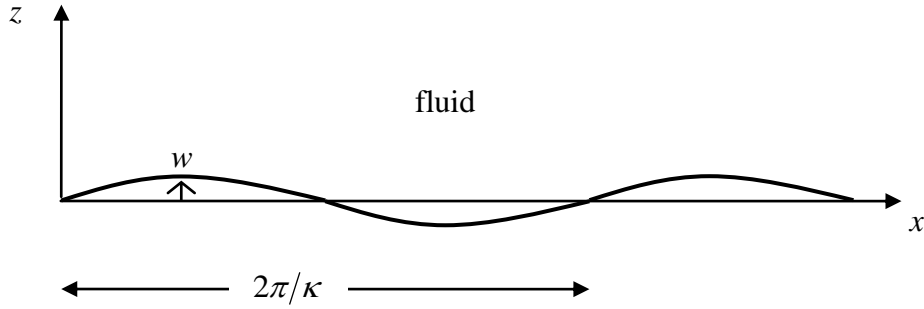


Figure 3.1. Transverse wave in a plate in contact with a fluid.

The appropriate sign of the square root in Eq. (3.3) depends on the values of  $k$  and  $\kappa$ . For the case  $\kappa \leq k$ , a real  $k_z$  is obtained and plane sound waves will travel away from the plate surface with  $k_z \geq 0$ . Meanwhile for the case  $\kappa > k$  an imaginary  $k_z$  is obtained which can be conveniently expressed as  $k_z = -i(\kappa^2 - k^2)^{1/2}$ . In the latter case, the disturbance of the fluid decays exponentially with the distance normal to the plate. For the opposite sign it would grow exponentially which is not allowed as a solution. Therefore in the plate-fluid interaction, propagating sound waves only exist due to the plate wave when  $\kappa < k$ . In other words the plate wave phase speed must be greater than the sound wave phase speed (supersonic velocity) in order to radiate energy into the far field.

The radiated pressure field caused by the plate vibration can then be calculated by the use of the specific acoustic wave impedance  $z_a$  which is defined as the ratio of the complex amplitudes of pressure and normal particle velocity. At the plate-fluid interface, the particle velocity in the  $z$ -direction  $v_z$  is equal to the surface normal velocity of the plate  $v$ . Hence [1]

$$z_a = \left( \frac{p}{v_z} \right)_{z=0} = \frac{\omega \rho_0}{k_z} = \frac{\rho_0 c k}{(k^2 - k_x^2)^{1/2}} \quad (3.4)$$

where  $p$  is the pressure amplitude,  $v_z$  is the particle velocity in the  $z$ -direction,  $\rho_0$  is the fluid density.

Using the spatial Fourier transform, an arbitrary velocity distribution  $v(x)$  can be transformed into the wavenumber domain using

$$\tilde{V}(k_x) = \int_{-\infty}^{\infty} v(x) e^{ik_x x} dx \quad (3.5)$$

and its inverse Fourier transform

$$v(x) = \frac{1}{2\pi} \int_{-\infty}^{\infty} \tilde{V}(k_x) e^{-ik_x x} dk_x \quad (3.6)$$

A similar expression can be written for the sound pressure. Therefore, from Eq. (3.4) the sound pressure at  $z = 0$  can be expressed in the wavenumber domain as

$$[\tilde{P}(k_x)]_{z=0} = z_a(k_x) \tilde{V}(k_x) = \frac{\rho_0 c k}{(k^2 - k_x^2)^{1/2}} \tilde{V}(k_x) \quad (3.7)$$

### 3.2 Plate strip

Now, consider a simply supported plate strip of infinite length (in the  $x$ -direction) and of finite width (in the  $y$ -direction) vibrating harmonically in an infinite rigid baffle. The vibration of the plate surface and the resulting pressure can be written as a two dimensional Fourier transform analogous to Eq. (3.6) as follows

$$v(x, y) = \frac{1}{4\pi^2} \int_{-\infty}^{\infty} \int_{-\infty}^{\infty} \tilde{V}(k_x, k_y) e^{-i(k_x x + k_y y)} dk_x dk_y \quad (3.8)$$

$$[p(x, y)]_{z=0} = \frac{1}{4\pi^2} \int_{-\infty}^{\infty} \int_{-\infty}^{\infty} [\tilde{P}(k_x, k_y)]_{z=0} e^{-i(k_x x + k_y y)} dk_x dk_y \quad (3.9)$$

where  $k_x$  and  $k_y$  are the wavenumbers in the  $x$  and  $y$  directions.

The power radiated by the plate strip is given by

$$W_{rad} = \frac{1}{2} \text{Re} \left\{ \int_{-\infty}^{\infty} \int_{-\infty}^{\infty} p(x, y) v^*(x, y) dx dy \right\} \quad (3.10)$$

where  $*$  indicates the complex conjugate. By substituting Eq. (3.8)-(3.9) into Eq. (3.10), this gives

$$W_{rad} = \frac{1}{32\pi^4} \text{Re} \left\{ \int_{-\infty}^{\infty} \int_{-\infty}^{\infty} \left[ \int_{-\infty}^{\infty} \int_{-\infty}^{\infty} \left[ \tilde{P}(k_x, k_y) \right]_{z=0} e^{-i(k_x x + k_y y)} dk_x dk_y \right. \right. \\ \left. \left. \times \int_{-\infty}^{\infty} \int_{-\infty}^{\infty} V^*(k'_x, k'_y) e^{i(k'_x x + k'_y y)} dk'_x dk'_y \right] dx dy \right\} \quad (3.11)$$

where  $k'_x$  and  $k'_y$  are introduced to distinguish between the integration over  $k_x$  and  $k_y$  related to  $\tilde{P}$  and  $\tilde{V}$ . Referring to Eq. (3.7), the surface pressure for the two dimensional case can be replaced by the plate velocity distribution in two dimensions multiplied by the wave impedance, as follows

$$W_{rad} = \frac{1}{32\pi^4} \text{Re} \left\{ \int_{-\infty}^{\infty} \int_{-\infty}^{\infty} \left[ \int_{-\infty}^{\infty} \int_{-\infty}^{\infty} \frac{\rho_0 c k}{(k^2 - k_x^2 - k_y^2)^{1/2}} \tilde{V}(k_x, k_y) e^{-i(k_x x + k_y y)} dk_x dk_y \right. \right. \\ \left. \left. \times \int_{-\infty}^{\infty} \int_{-\infty}^{\infty} \tilde{V}^*(k'_x, k'_y) e^{i(k'_x x + k'_y y)} dk'_x dk'_y \right] dx dy \right\} \quad (3.12)$$

Further simplification can be made using the Dirac delta function in Eq. (2.23).

Therefore Eq. (3.12) can be simplified as

$$W_{rad} = \frac{1}{8\pi^2} \text{Re} \left\{ \int_{-\infty}^{\infty} \int_{-\infty}^{\infty} \frac{\rho_0 c k}{(k^2 - k_x^2 - k_y^2)^{1/2}} |\tilde{V}(k_x, k_y)|^2 dk_x dk_y \right\} \quad (3.13)$$

where  $|\tilde{V}(k_x, k_y)|^2$  is the square of the plate velocity in the wavenumber domain. It is possible to limit consideration to wavenumbers satisfying the necessary condition for

plate waves to be able to radiate sound energy, that is  $k_x^2 + k_y^2 \leq k^2$ ; elsewhere the term  $(k^2 - k_x^2 - k_y^2)^{1/2}$  is imaginary. Therefore, the range of integration can be limited to give

$$W_{rad} = \frac{\rho_0 c}{8\pi^2} \int_{-k}^k \int_{-\sqrt{k^2 - k_x^2}}^{\sqrt{k^2 - k_x^2}} \frac{k}{(k^2 - k_x^2 - k_y^2)^{1/2}} |\tilde{V}(k_x, k_y)|^2 dk_x dk_y \quad (3.14)$$

### 3.2.1 Radiation due to point force

The normal velocity distribution  $v(x, y)$ <sup>1</sup> due to the point force can be found from the displacement solution in section 2.3 using

$$v(x, y) = i\omega w(x, y) \quad (3.15)$$

where  $w(x, y)$  is the surface displacement of the plate strip which is given by Eq. (2.14). Now the normal surface velocity is

$$v(x, y) = \sum_{m=1}^{\infty} \frac{\omega F_m}{2D'k_{x1,m}(k_{x1,m}^2 - k_{x2,m}^2)} \left( e^{-ik_{x1,m}|x|} - \frac{k_{x1,m}}{k_{x2,m}} e^{-ik_{x2,m}|x|} \right) \sin\left(\frac{m\pi y}{l_y}\right) \quad (3.16)$$

The modulus squared  $|\tilde{V}(k_x, k_y)|^2$  of Eq. (2.20), which reflects the energy spectrum of  $\tilde{V}(k_x, k_y)$ , is given by

$$|\tilde{V}(k_x, k_y)|^2 = \left| \frac{\omega F_m}{D'(k_{x1,m}^2 - k_x^2)(k_{x2,m}^2 - k_x^2)} \right|^2 \left[ \frac{2\pi m / l_y}{k_y^2 - (m\pi / l_y)^2} \right]^2 \sin^2\left(\frac{k_y l_y - m\pi}{2}\right) \quad (3.17)$$

For the time being, it is assumed that each transverse order  $m$  of the transverse velocity  $\tilde{V}(k_x, k_y)$  radiates sound independently, i.e. cross terms are ignored for simplicity. This allows the radiated power of the plate strip due to a point force excitation to be expressed as

---

<sup>1</sup> Note that some publications use index  $n$  for the variable  $v$  to indicate the velocity in the normal direction  $v_n$ . In this report, it does not appear explicitly but the velocity  $v$  is actually the velocity distribution in the  $z$ -direction so that this is the normal velocity.

$$W_{rad} = \frac{\rho_0 c}{8\pi^2} \sum_{m=1}^{\infty} \int_{-k}^k \int_{-\sqrt{k^2-k_y^2}}^{\sqrt{k^2-k_y^2}} \frac{k}{(k^2 - k_x^2 - k_y^2)^{1/2}} \left| \frac{\omega F_m}{D'(k_{x1,m}^2 - k_x^2)(k_{x2,m}^2 - k_x^2)} \right|^2 \left[ \frac{2\pi m / l_y}{k_y^2 - (m\pi/l_y)^2} \right]^2 \sin^2 \left( \frac{k_y l_y - m\pi}{2} \right) dk_x dk_y \quad (3.18)$$

Note that the radiated sound power can be determined using a different approach e.g. Junger and Feit [6] and Sakagami et al. [7] use a far-field solution to calculate the radiated power of a plate strip or waveguide structure.

The radiation ratio  $\sigma$  is used to indicate how much sound power is radiated on the basis of the actual vibrating surface compared with the infinite flat surface vibrating in phase with the same mean-square velocity. It is thus defined as [1, 2, 8, 9]

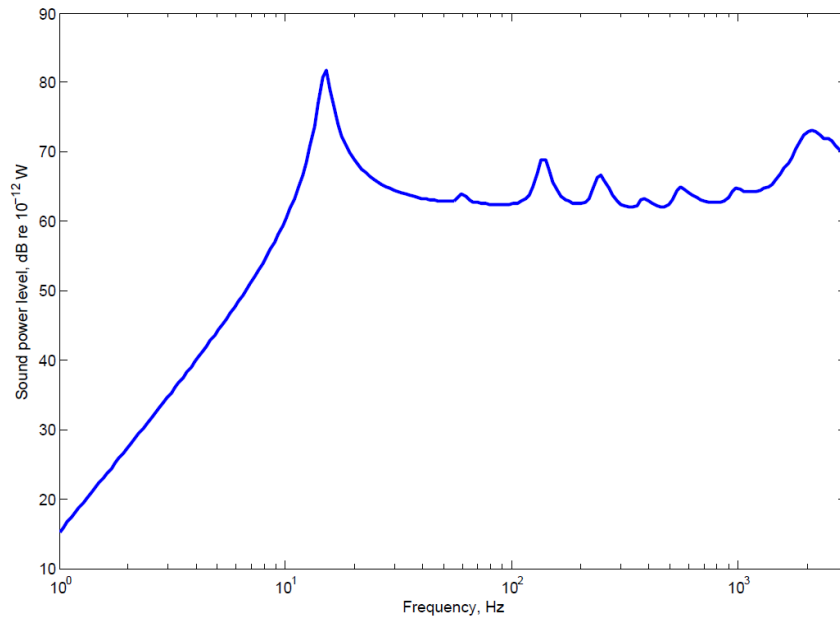
$$\sigma = \frac{W_{rad}}{\rho_0 c S \langle v^2 \rangle} \quad (3.19)$$

where  $\rho_0$  is the fluid density,  $c$  is the sound velocity,  $S$  is the surface area and  $\langle v^2 \rangle$  is the spatially averaged mean-square velocity. For the plate strip case, the ‘average’ is an integral over the  $x$  - direction so the area is replaced by the width  $l_y$  :

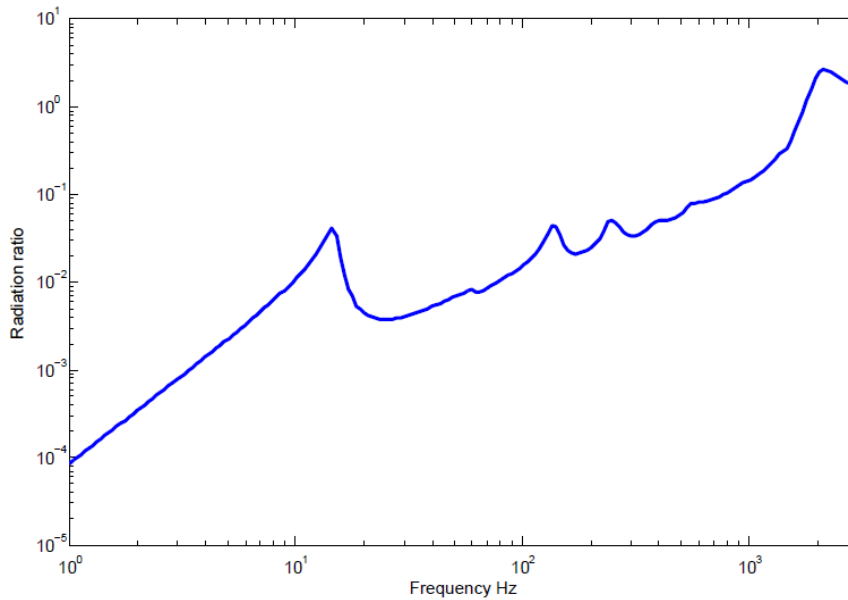
$$\sigma = \frac{W_{rad}}{\rho_0 c l_y \langle v^2 \rangle_{inf}} \quad (3.20)$$

where  $\langle v^2 \rangle_{inf}$  now represents the integral of the mean-square velocity over the length and the average over the width.

Figure 3.2 presents the radiated sound power and radiation ratio of the plate strip considered in the previous section due to a point force excitation at position  $(0, 0.433 l_y)$ . The total number of modes  $M = 81$  is the same as used in the mobility calculation in section 2.3. The radiated power has peaks at the various cut-on frequencies. The critical frequency is 2 kHz at which the radiation ratio reaches its maximum value.



(a)



(b)

Figure 3.2. (a) Sound power radiation of the plate strip due to a unit point force at  $(0, 0.433l_y)$ ; (b) its associated radiation ratio.

### 3.2.2 Effect of finiteness and point force excitation on the plate strip

It is interesting to see the effect of the finite plate width and the effect of the point force excitation in the case of the plate strip. The plate strip differs from an infinite plate, on the one hand, and a finite plate on the other hand. In the infinite plate above the critical frequency  $f_c$ , sound is radiated effectively by the plate vibration.

However, as seen in section 3.1 there is no radiated power from a plane wave in an infinite plate below the critical frequency because of acoustic short-circuiting. For a point force excitation radiation will occur from the nearfield in the vicinity of the forcing point. In contrast, a finite plate experiences non-zero radiation below the critical frequency due to the influence of edges and corners [10]. The plate strip has a finite width but infinite length which makes the problem more complex, especially for the case below the critical frequency.

In principle, referring to [1, 4], whenever the trace wavenumber in a particular direction in a structure is higher than the acoustic wavenumber  $k$  at the same frequency, acoustic short-circuiting will occur. In the case under consideration, the acoustic short-circuiting occurs when the characteristic wavenumber in the  $y$  direction  $k_y = m\pi/l_y$  is higher than the acoustic wavenumber  $k$  i.e.  $(m\pi/l_y > k)$ . Under this circumstance, because the adjacent anti-nodal regions in the plate strip are separated by much less than the acoustic wavelength in the surrounding medium, the fluid displaced outward by one region will compensate for the inward motion in the adjacent region[10]. However, the finite width of the structure means that the acoustic short-circuiting is incomplete at the edges. The combination of  $(m\pi/l_y > k)$  and the structural wavenumbers in the  $x$  - direction which are smaller than the acoustic wavenumber  $(k_{x1,m} < k)$  would create radiating modes along the edge in the  $x$  - direction. Commonly, on a finite plate such modes are termed edge modes.

The acoustic short-circuiting is also present in the  $x$  - direction. When the condition  $k_{x1,m} > k$  is fulfilled, the cancellation takes place completely along the plate as it is infinite in length. Hence only the radiating component due to the nearfield wave and the discontinuity introduced by the point force exist. This means neither edge modes nor corner modes are found in this direction. However, not all free propagating waves undergo the short-circuiting because this depends on the mode order, which determines the wavenumbers  $k_{x1,m}$  and  $k_{x2,m}$ . As mentioned in section 2.1,  $k_{x1,m}$  relates to the propagating waves which carry vibration energy above their cut-on frequencies while  $k_{x2,m}$  corresponds to the nearfield waves. As shown by the dispersion curves of the plate strip in Figure 3.3, in this example only the first five propagating waves have wavenumbers higher than the acoustic wavenumber  $k$ . The

rest of the modes have wavenumbers that are lower than the acoustic wavenumbers ( $k_{x1,m} < k$ ) and hence contribute to the sound power radiation. Peaks are associated with the cut-on frequency behaviour for every mode order  $m$  as all the dispersion curves start below the diagonal line representing  $k$ .

To provide a visual description of the radiation components of the plate strip, a classification can be made intuitively by considering the wavenumber distribution over the frequency range of interest. Figure 3.3 presents dispersion curves corresponding with the wavenumbers in the  $x$ -direction  $k_{x1,m}$  and primary wavenumber components<sup>2</sup> in the  $y$ -direction  $k_y = m\pi/l_y$  respectively with the absence of the damping loss factor. The acoustic wavenumber values and an indication of the critical frequency are added to each graph to help identifying the various regions where the radiation components can be described based on their values relative to the acoustic wavenumber  $k$ . Regions A and B indicate regions in which  $k_{x1,m} > k$  and  $k_{x1,m} < k$  respectively. Meanwhile, regions C and D are assigned for the corresponding wavenumber area for  $k_y$ . Hence,  $k_y > k$  occupies the region C and  $k_y < k$  can be found in region D. Following the explanations from the previous paragraphs, some combinations of these regions can thus be identified as follows

1. The combination of regions A and C causes a zero radiation ratio as there are no corner modes present due to the complete acoustic short-circuiting along the infinite direction.
2. The combination of regions A and D leads to a similar situation. The structural wavenumber in the  $y$ -direction is smaller than the acoustic one would result in radiation. However, there is a complete short-circuiting along the  $x$ -direction, hence a zero radiation occurs.
3. The combination of regions B and C clearly leads to the edge modes along the  $x$ -direction where the acoustic short-circuiting takes place along the direction normal to this axis.

---

<sup>2</sup> It should be borne in mind that the finite extent over width produces modal wavenumber spectra with the spectrum peaks found at  $(m\pi/l_y)$  rather than single wavenumber as found in an infinite plate. Therefore, in this study,  $k_y = m\pi/l_y$  is termed the primary wavenumber. The same terminology is also found in [1].

4. The combination of regions B and D is related to surface radiation component where the radiation ratio tends to unity at high frequency. Note that region B and D can occur below  $f_c$  but mostly occurs above this frequency.

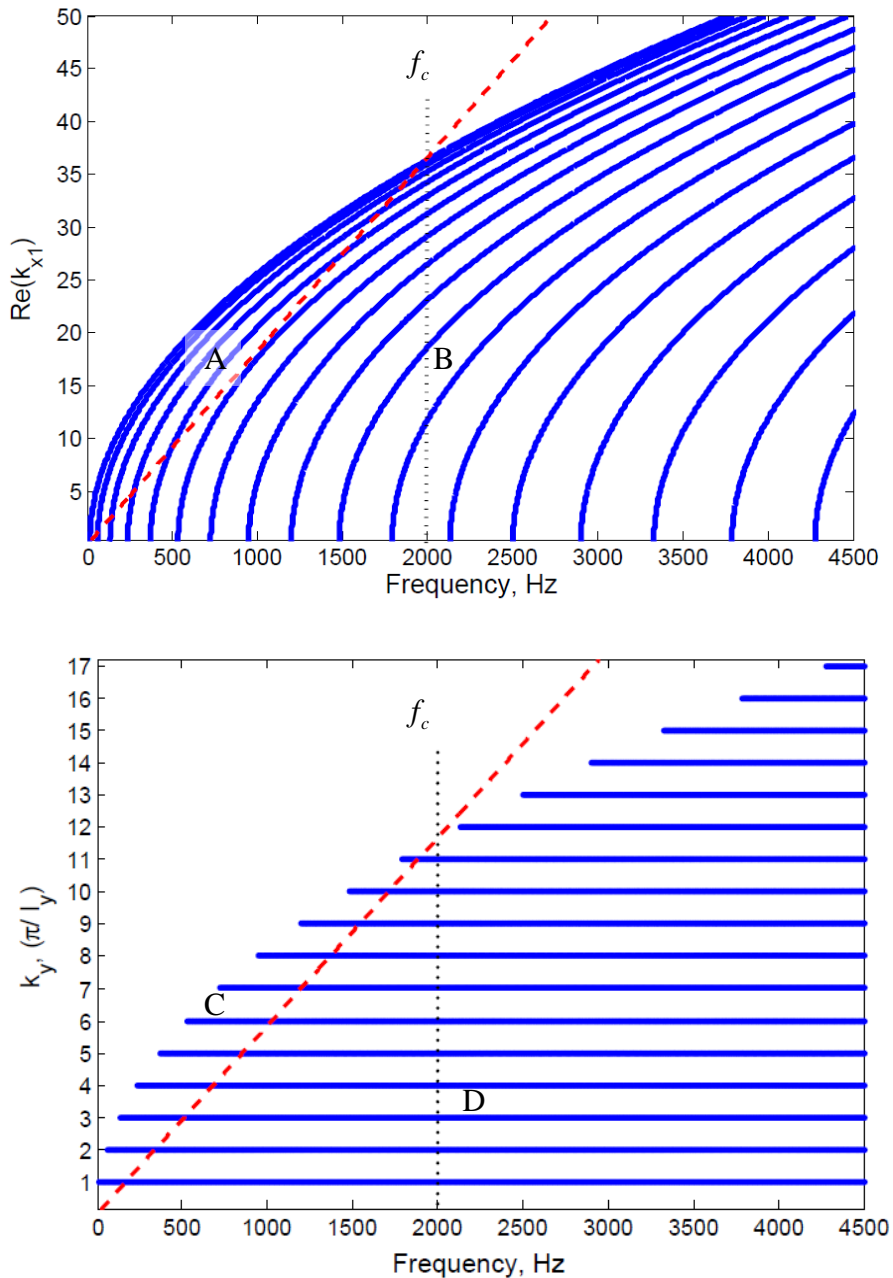


Figure 3.3. Dispersion curve of the plate strip (— bending wavenumbers for different mode orders ( $k_{x1}$ ) and wavenumber for each mode  $m$  ( $k_y$ ); - - - acoustic wavenumbers).

Figure 3.4 compares the radiated power of the plate strip and the infinite plate. The radiated power of the infinite plate due to a point force  $W_{\text{inf}}$  was calculated based on a formulation proposed in [2] but neglecting the fluid loading contribution as follows

$$W_{\text{inf}} = \frac{F_0^2 \rho_0 c k}{4\pi} \int_0^k \frac{k_r dk_r}{\sqrt{k^2 - k_r^2} \left[ (\omega \rho h)^2 \left(1 - k_r^4 / k_B^4\right)^2 \right]} \quad (3.21)$$

where  $k_r^2 = k_x^2 + k_y^2$ . If the frequency range of interest is limited to well below the critical frequency ( $k_r \ll k_B$ ) so that  $(1 - k_r^4 / k_B^4) \approx 1$ , this gives

$$W_{\text{inf}} = \frac{F_0^2 \rho_0 c k}{4\pi (\omega \rho h)^2} \int_0^k \frac{k_r dk_r}{\sqrt{k^2 - k_r^2}} = \frac{F_0^2 \rho_0}{4\pi c (\rho h)^2} \quad (3.22)$$

which is independent of frequency.

It is clear that the radiated power of the plate strip is higher than the infinite plate result for frequencies above the first cut-on frequency and below the critical frequency. The presence of the edge mode radiation component has caused more power to be radiated compared with the infinite plate for the same amplitude of force. Conversely, only the radiated power of the nearfield around the forcing position can be found from the infinite plate for this frequency region. Below the first cut-on frequency, the radiated power of the plate strip is less than that of the infinite plate as the stiffness characteristic of the plate strip determines its radiated power whereas in this frequency region that of the infinite plate depends on the square of the mass per unit area as indicated in Eq. (3.22). Above the critical frequency the results of both models are similar.

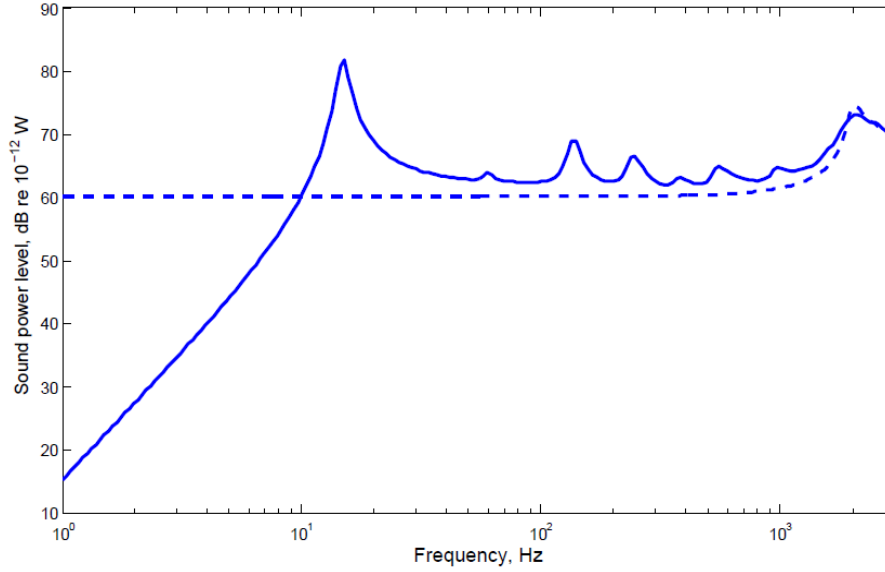


Figure 3.4. Radiated power of plate strip and infinite plate excited at position  $(0, 0.433l_y)$  with force amplitude  $F_0 = 1$  (— plate strip; --- infinite plate).

### 3.2.3 Effect of damping loss factor

Figure 3.5 indicates the effect of the damping loss factor on the radiated sound power. In general, its effect mostly appears at the cut-on frequencies at which the peak amplitude increases as the damping loss factor decreases. However, the effect significantly increases at the frequencies where there are several bending wavenumbers which are lower than the acoustic wavenumbers i.e. above about 500 Hz (see Figure 3.3). In contrast, at low frequencies where the bending wavenumbers are generally higher than the acoustic wavenumbers for most frequencies, the damping only affects the radiated power close to the cut-on frequencies. In this lower frequency region, away from the cut-on frequencies, only a small part of the vibration, which corresponds to nearfield or evanescent waves, radiates into the fluid medium. Therefore, as the nearfield is almost independent of the damping values, the damping loss factor has a negligible effect in this region except at the cut-on frequencies [2].

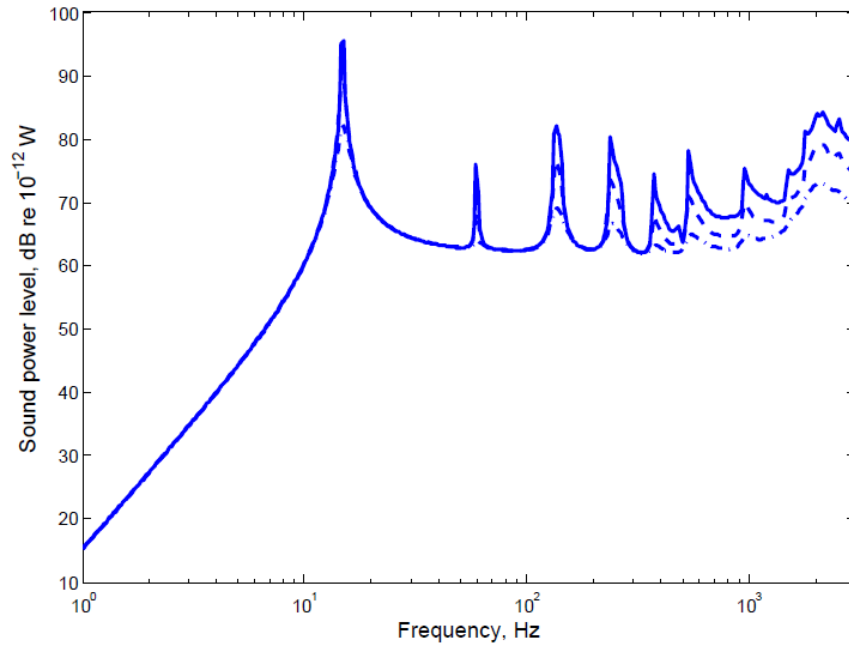


Figure 3.5. Comparison of sound power radiation for different damping loss factors for plate strip excited at  $(0, 0.433l_y)$  (—  $\eta = 0.01$  ; ---  $\eta = 0.03$ ; -·-·  $\eta = 0.1$ ).

The corresponding radiation ratios are shown in Figure 3.6. The greatest damping effect is found in the acoustic short-circuiting region while the effect is negligible at frequencies below the first cut-on frequency and above the critical frequency. It is clear that the radiation ratio in the short-circuiting region is proportional to the damping value as the average mean-square velocity decreases with increasing damping (see section 2.3.7).

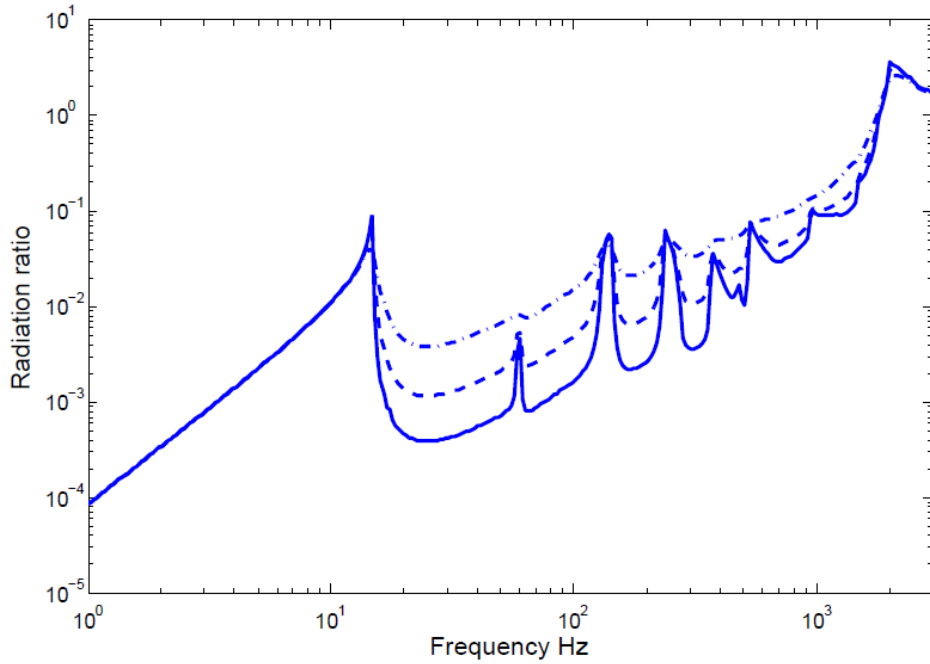
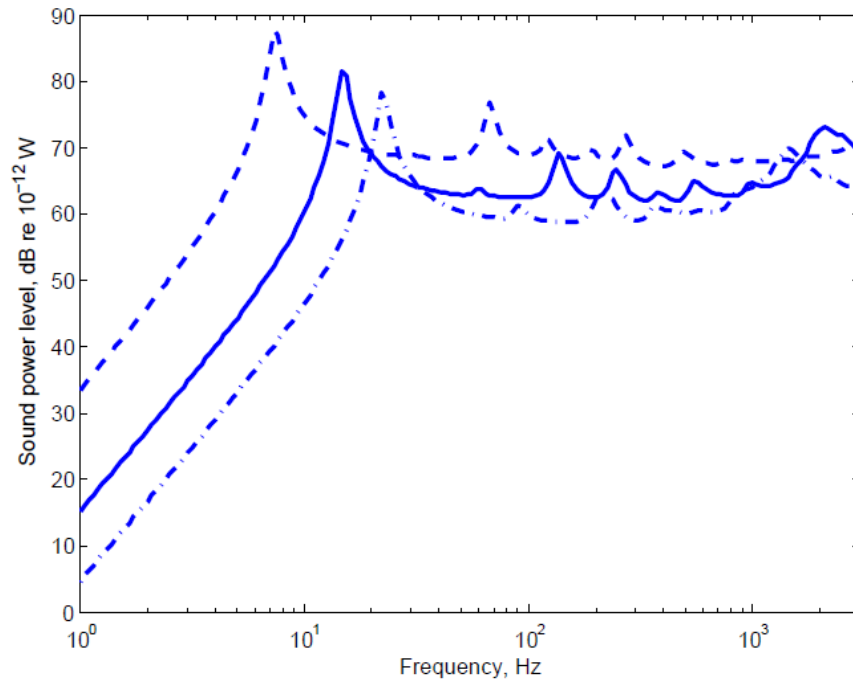


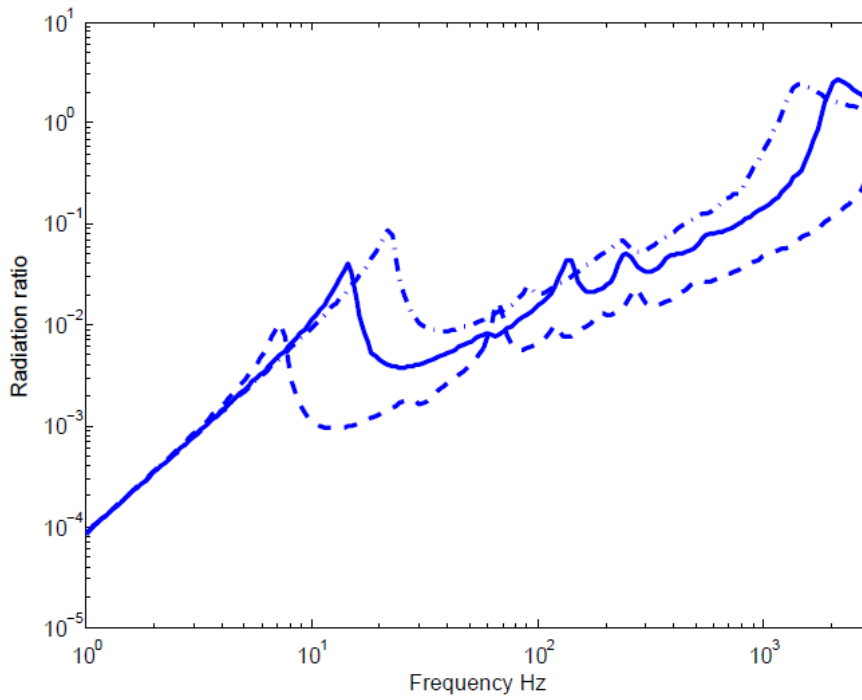
Figure 3.6 Comparison of radiation ratio due to different damping loss factor excited at  $(0, 0.433l_y)$  (—  $\eta = 0.01$  ; ---  $\eta = 0.03$ ; -·-·  $\eta = 0.1$ ).

### 3.2.4 Effect of plate thickness

The effect of the plate thickness can be observed from Figure 3.7(a). It is clear that the sound power level increases across the frequency range considered as the thickness of the plate strip is reduced. Moreover, the first cut-on frequency is reduced and the critical frequency is increased as the thickness reduces. Therefore the frequency region between the first cut-on frequency and the critical frequency becomes wider and the acoustic short-circuiting effect is increased. This is seen in the radiation ratio which is plotted in Figure 3.7(b). The radiation ratio decreases as the thickness reduces in the acoustic short-circuit region. Below the first cut-on frequency and above the critical frequency the radiation ratio is largely unaffected.



(a)



(b)

Figure 3.7. (a) Comparison of sound power radiation due to different thickness with damping loss factor equal to 0.1 and excited at  $(0, 0.433 l_y)$ ; (b) its associated radiation ratio ( $- - - h = 3 \text{ mm}$ ;  $- h = 6 \text{ mm}$ ;  $- \cdot - \cdot h = 9 \text{ mm}$ ).

### 3.2.5 Inclusion of the cross-terms

In the formulation of the previous section, the radiated sound power is calculated on the basis of individual modes generating sound independently. In fact, there is an interaction between the resulting pressures produced by one mode of a vibrating structure and vibration of other modes. Hence it is of importance to assess the cross-term contributions to the resulting radiated sound power. This has been studied in [11] for a finite plate where it is shown that neglecting the cross modal contribution can lead to under- or over-estimates of the radiated power even at resonance frequencies. They are frequently disregarded in the radiated power formulation due to the computational burden they introduce in calculation.

To include the cross-terms in the radiated sound power formulation, Eq. (3.18) needs to be modified. It becomes

$$W_{rad} = \frac{\rho_0 c}{8\pi^2} \sum_{m=1}^{\infty} \sum_{m'=1}^{\infty} \int_{-k}^k \int_{-\sqrt{k^2-k_y^2}}^{\sqrt{k^2-k_y^2}} \frac{k}{(k^2 - k_x^2 - k_y^2)^{1/2}} \tilde{V}_m(k_x, k_y) \tilde{V}_{m'}^*(k_x, k_y) dk_x dk_y \quad (3.23)$$

where  $\tilde{V}_m$  and  $\tilde{V}_n$  are defined by Eq. (2.20) with  $m$  and  $m'$  the mode index of velocity corresponding to pressure and velocity respectively.

Figure 3.8 presents a comparison of the radiated power calculated with only self-modal radiation and including the cross modal radiation using the same material properties as listed in Table 2.1 with excitation at position  $(0, 0.433l_y)$ . It is clear that the cross-terms contribute to the radiated sound power mainly away from the cut-on frequencies in the acoustic short circuiting region between the first cut-on frequency and the critical frequency. Below the first cut-on frequency and around the critical frequency, both formulations agree well.

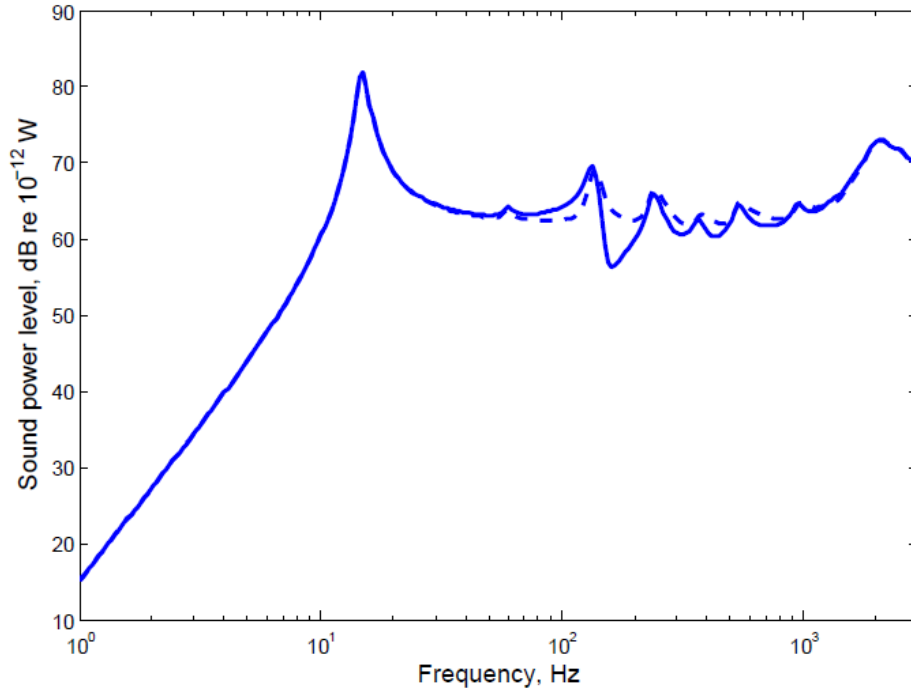


Figure 3.8. Effect of the cross-terms contribution in radiated power due to a point force excitation at  $(0, 0.433 l_y)$  (— the cross-terms modal radiation incorporated along with the self-modal one ; --- only self- modal radiation considered).

As pointed out earlier, the resulting radiated power using Eq. (3.23) increases calculation time considerably. Using Matlab on a personal computer powered by an Intel Pentium Quadcore 2.8 GHz processor and 4 Gbyte memory, it requires 24.6 hours to get the result. This is around 78 times the calculation time required to obtain the results where the cross-term contribution is neglected.

### 3.3 Summary

Unlike an infinite plate, a plate strip still radiates sound at frequencies below its critical frequency due to the finite extent in one dimension. Therefore, edge modes effectively contribute to the radiated sound power even though the wavenumbers in the  $y$  - direction,  $k_y$ , are higher than the acoustic wavenumber in this frequency region. In the infinite dimension, that is in the  $x$  - direction, the radiated power is also present at frequencies below the critical frequency when  $k_{x1,m} < k$ . For the opposite condition sound radiation occurs which is only significant in the area close to the

excitation position. Peaks found in the radiated power curve are associated with the cut-on frequencies which always have  $k_{x1,m} \ll k$ .

The greatest effect of damping on the radiated sound power appears at the cut-on frequencies. The damping also has a broadband effect for higher frequencies at which the bending wavenumbers  $k_{x1,m}$  are lower than the acoustic wavenumbers  $k$ . Considering the related radiation ratio, it is clear that the damping loss factor affects the results significantly in the acoustic short-circuiting region between the first cut-on frequency and the critical frequency.

A thicker plate strip will radiate less power as the average mean-square velocity reduces for a thicker plate. On the other hand it will reduce the frequency range of the acoustic short-circuiting area which increases the radiation ratio.

## 4. Sound transmission loss of a plate strip

In this section the sound transmission due to a plane acoustic wave acting on the simply supported plate strip (waveguide) is considered. The incident plane wave impinges on the plate strip with elevation angle  $\theta$  and azimuth angle  $\varphi$  as shown in Figure 4.1. The sound transmission loss (STL) is determined by considering the bending waves in the plate. The bending stiffness therefore influences the STL calculation inherently. Moreover, the finite width and the boundary conditions of the plate strip on its two edges are expected to give useful insights of those effects in the transmission loss prediction where they are not considered explicitly in most classical theory based on infinite plates, e.g. in Ref. [1, 10, 12].

### 4.1 Pressure and velocity functions

Since the structure is finite in the  $y$ -direction a modal solution can be utilized to describe the structural response in terms of  $y$  as in section 2. Meanwhile, for the  $x$ -direction, as the structure is infinite, a travelling wave solution is suitable to describe the dependence of displacement on  $x$ . Therefore, the general solution for the radiated pressure  $p$  and the plate velocity  $v$  can be decomposed into terms of the form

$$p(x, y) = p_m e^{-i\kappa x} \sin\left(\frac{m\pi y}{l_y}\right), \quad v(x, y) = v_m e^{-i\kappa x} \sin\left(\frac{m\pi y}{l_y}\right) \quad (4.1)$$

where  $m$  is an integer and  $\kappa$  is the (real) wavenumber in the  $x$ -direction.

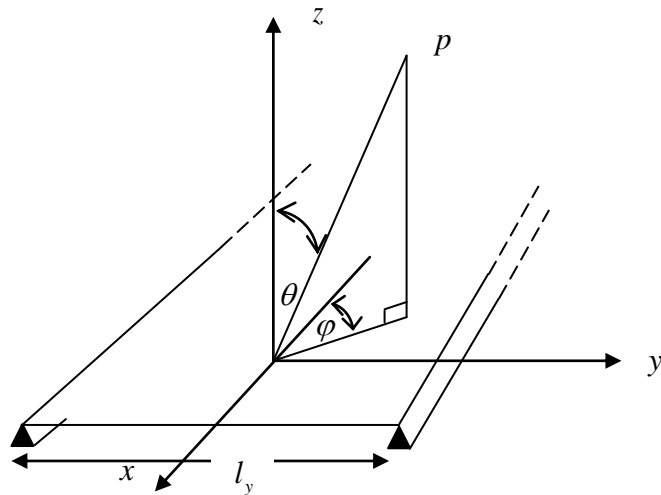


Figure 4.1. Direction of a plane wave incident on an infinite plate strip

Before proceeding to the mathematical formulation and solution for the transmission coefficient, some simplifying assumptions should be noted as follows:

1. As in previous sections, the plate strip is modelled with the thin-plate theory and it is set in a rigid baffle.
2. The thickness of the baffle and the plate is neglected.
3. The amplitude of the reflected sound pressure is initially assumed equal to the incident sound pressure so that the blocked pressure field at the plate surface is equal to twice the incident pressure.
4. Simply supported boundaries are assumed.
5. The acoustic medium on both sides of the plate is assumed to be identical.

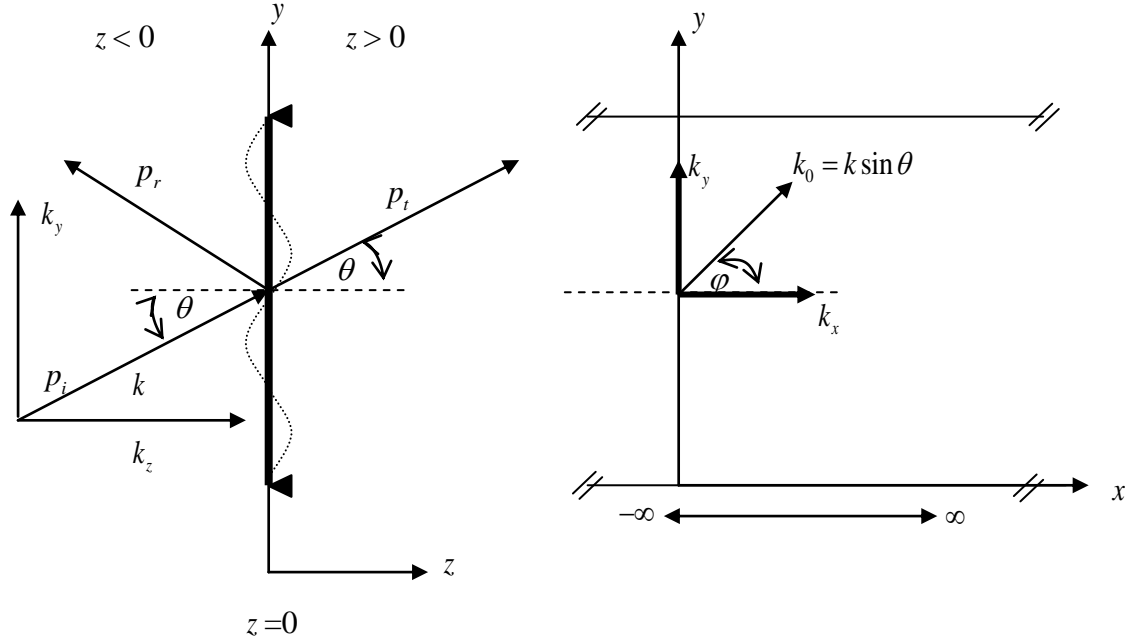


Figure 4.2. Elevation and azimuth angle convention and trace wavenumbers in the fluid.

Considering Figure 4.2 the incident sound pressure is considered as a plane wave expressed by

$$p_i(x, y, z) = p_i e^{-ik_x x} e^{-ik_y y} e^{-ik_z z} \quad (4.2)$$

where time harmonic dependence  $e^{i\omega t}$  is omitted for clarity. The wavenumbers in  $x$ ,  $y$  and  $z$  directions can be defined as follows:

$$\begin{aligned} k_z &= k \cos \theta \\ k_x &= k \sin \theta \cos \varphi \\ k_y &= k \sin \theta \sin \varphi \end{aligned} \quad (4.3)$$

where  $k = \sqrt{k_x^2 + k_y^2 + k_z^2}$  is given by  $k = \omega/c$  with  $\omega$  the angular frequency and  $c$  the sound velocity.

For a rigid, uniform and infinitely extended plate, the pressure field in  $z < 0$  (the source side) consists of the superposition of the incident wave and a reflected

wave. At the plate surface they add in phase to give the so-called blocked pressure  $p_{bl}$ . When the plate motion is considered, the plate radiates in the negative and positive  $z$ -directions. The radiated pressure in the positive  $z$ -direction is then called the transmitted sound pressure  $p_t$ . The total pressure on the plate surface at  $z=0$  consists of the superposition of the blocked pressure field and the radiated pressure field on both sides of the plate. The radiated pressure terms in the total pressure will impose a fluid loading at the plate surface. An implication of this is that it will introduce a damping to the plate strip in addition to the internal damping loss factor. Due to the finite width, the radiated field on either side of the plate strip does not consist of a plane wave.

The two-dimensional bending wave equation subject to the applied acoustic pressure field and the radiated acoustic pressure produced by the plate velocity is

$$D' \left( \left( \frac{\partial^4 v}{\partial x^4} + 2 \frac{\partial^4 v}{\partial x^2 \partial y^2} + \frac{\partial^4 v}{\partial y^4} \right) - k_B^4 v \right) = i\omega (p_{bl} + p_{rad}^- - p_{rad}^+) \quad (4.4)$$

The distribution of the pressure  $p(x, y)$  may be expressed by the combination of a Fourier integral and a Fourier series. This yields

$$p(x, y) = \frac{1}{2\pi} \int_{-\infty}^{\infty} \sum_{m=1}^{\infty} p_m(\kappa) e^{-i\kappa x} \sin\left(\frac{m\pi y}{l_y}\right) d\kappa \quad (4.5)$$

and

$$p_m(\kappa) = \frac{2}{l_y} \int_0^{l_y} \int_{-\infty}^{\infty} p(x, y) e^{i\kappa x} \sin\left(\frac{m\pi y}{l_y}\right) dx dy \quad (4.6)$$

where  $m$  is an integer corresponding to each mode of the pressure in the  $y$ -direction and  $\kappa$  is the (real) wavenumber in the  $x$ -direction.

As stated earlier, it is assumed that a blocked reflected sound pressure is generated equal to the incident sound pressure at the plate surface. The total pressure on the plate surface at  $z=0$  consists of the superposition of the blocked pressure field and the radiated pressure field due to plate motion on both sides of the plate. Hence the pressure for mode  $m$  is given by

$$p(x, y) = 2p_i e^{-ik_y y} e^{-ik_x x} + (p_{rad}^-(y) - p_{rad}^+(y)) e^{-ik_x x} \quad (4.7)$$

and Eq. (4.6) becomes

$$p_m = \frac{2}{l_y} \int_0^{l_y} (2p_i e^{-ik_y y} + p_{rad}^-(y) - p_{rad}^+(y)) \sin\left(\frac{m\pi y}{l_y}\right) dy \left( \int_{-\infty}^{\infty} e^{i(\kappa - k_x)x} dx \right) \quad (4.8)$$

It may be noted that  $\int_{-\infty}^{\infty} e^{i(\kappa - k_x)x} dx = 2\pi\delta(\kappa - k_x)$ . Hence

$$p(x, y) = \sum_{m=1}^{\infty} A_m \sin\left(\frac{m\pi y}{l_y}\right) e^{-ik_x x} \quad (4.9)$$

where

$$A_m = \frac{2}{l_y} \int_0^{l_y} (2p_i e^{-ik_y y'} + p_{rad}^-(y') - p_{rad}^+(y')) \sin\left(\frac{m\pi y'}{l_y}\right) dy' \quad (4.10)$$

Similarly, because the plate strip is uniform and infinite in the  $x$ -direction, its transverse velocity may be written in the form

$$v(x, y) = \frac{1}{2\pi} \int_{-\infty}^{\infty} \sum_{m'=1}^{\infty} v_{m'} e^{-ik_x x} \sin\left(\frac{m'\pi y}{l_y}\right) d\kappa \quad (4.11)$$

Using the same argument as above  $\int_{-\infty}^{\infty} e^{i(\kappa - k_x)x} dx = 2\pi\delta(\kappa - k_x)$  and hence

$$v(x, y) = \sum_{m'=1}^{\infty} v_{m'} \sin\left(\frac{m'\pi y}{l_y}\right) e^{-ik_x x} \quad (4.12)$$

where  $m'$  is an integer designating each mode of the plate vibration. Eq. (4.12) can be conveniently written as

$$v(x, y) = \sum_{m'=1}^{\infty} v_{y,m'}(y) e^{-ik_x x} \quad (4.13)$$

where  $v_{y,m'}(y) = v_{m'} \sin\left(\frac{m'\pi y}{l_y}\right)$ . This transverse velocity is only defined for  $0 \leq y \leq l_y$

and is zero otherwise. Subsequently, it can be expressed in terms of an infinite set of simple harmonic waves travelling in the  $y$ -direction, with wavenumber denoted as  $\gamma$  in order to distinguish it from the incident wavenumber  $k_y$ , as follows

$$\tilde{V}_{y,m'}(\gamma) = \int_0^{l_y} v_{y,m'}(y) e^{i\gamma y} dy \quad (4.14)$$

$$v_{y,m'}(y) = \frac{1}{2\pi} \int_{-\infty}^{\infty} \tilde{V}_{y,m'}(\gamma) e^{-i\gamma y} d\gamma \quad (4.15)$$

The solution for  $\tilde{V}_{y,m'}(\gamma)$  is

$$\tilde{V}_{y,m'}(\gamma) = v_{m'} a_{m'}(\gamma) \quad (4.16)$$

where  $a_{m'}(\gamma) = \int_0^{l_y} \sin\left(\frac{m'\pi y}{l_y}\right) e^{i\gamma y} dy = \frac{(m'\pi/l_y)[(-1)^{m'} e^{i\gamma l_y} - 1]}{[\gamma^2 - (m'\pi/l_y)^2]}$  (see also Eq. (2.20)).

In order to solve the coupled vibration-radiation problem, some conditions must be satisfied, i.e. the fluid particle velocity must be equal to the normal plate velocity and the fluid particle velocity  $v$  and the pressure  $p$  must satisfy Euler's equation  $i\omega\rho_0\vec{v} = -\vec{\nabla}p$ . Therefore, the (normal) plate velocity  $v$  in Eq. (4.13) is related to the radiated pressure by

$$v = -\frac{1}{i\omega\rho_0} \left. \frac{\partial p}{\partial z} \right|_{z=0} \quad (4.17)$$

Hence the radiated pressure field, assuming the fluid on both sides is the same, is

$$\begin{aligned} p_{rad}(x, y) &= \frac{1}{2\pi} \int_{-\infty}^{\infty} \sum_{m'=1}^{\infty} V_y(\gamma) e^{-i\gamma y} e^{-ik_x x} \left( \frac{\omega\rho_0}{k_z} \right) d\gamma \\ &= \frac{1}{2\pi} \int_{-\infty}^{\infty} \sum_{m'=1}^{\infty} v_{m'} a_{m'}(\gamma) e^{-i\gamma y} e^{-ik_x x} \left( \frac{\omega\rho_0}{k_z} \right) d\gamma \end{aligned} \quad (4.18)$$

or as a function of  $y$ , the radiated pressure can be written as

$$p_{rad}(y) = \frac{1}{2\pi} \int_{-\infty}^{\infty} \sum_{m'=1}^{\infty} v_{m'} a_{m'}(\gamma) e^{-i\gamma y} \left( \frac{\omega \rho_0}{k_z} \right) d\gamma \quad (4.19)$$

where  $k_z = \sqrt{k^2 - \kappa^2 - \gamma^2}$ . Note that  $p_{rad}^- = -p_{rad}^+$ .

Therefore,  $A_m$  in Eq.(4.10) becomes

$$\begin{aligned} A_m &= \frac{2}{l_y} \left( 2p_i a_m(k_y) - 2 \left[ \frac{1}{2\pi} \left( \int_{-\infty}^{\infty} \sum_{m'=1}^{\infty} v_{m'} a_{m'}(\gamma) \left( \frac{\omega \rho_0}{k_z} \right) d\gamma \right) \left( \int_0^{l_y} e^{-i\gamma y} \sin \left( \frac{m\pi y}{l_y} \right) dy \right) \right] \right) \\ &= \frac{2}{l_y} \left( 2p_i a_m(k_y) - \frac{1}{\pi} \left( \int_{-\infty}^{\infty} \sum_{m'=1}^{\infty} v_{m'} a_{m'}(\gamma) a_m^*(\gamma) \left( \frac{\omega \rho_0}{k_z} \right) d\gamma \right) \right) \end{aligned} \quad (4.20)$$

where  $a_m(-\gamma) = a_m^*(\gamma)$  as the modal displacement function is real.

Substituting Eq. (4.9) and Eq. (4.12) into Eq. (4.4), this gives

$$\sum_{m'=1}^{\infty} \left( -\frac{i}{\omega} \left[ D' \left( \left( k_x^2 + (m'\pi/l_y)^2 \right)^2 - k_B^4 \right) \right] \right) v_{m'} e^{-ik_x x} \sin \left( \frac{m'\pi y}{l_y} \right) = \sum_{m=1}^{\infty} A_m e^{-ik_x x} \sin \left( \frac{m\pi y}{l_y} \right) \quad (4.21)$$

Using the orthogonality of the mode shapes

$$\int_0^{l_y} \sin \left( \frac{m\pi y}{l_y} \right) \sin \left( \frac{m'\pi y}{l_y} \right) dy = \begin{cases} 0 & m \neq m' \\ \frac{l_y}{2} & m = m' \end{cases} \quad (4.22)$$

Eq. (4.21) can be written for a single term in the series; to obtain this, it is multiplied with  $\sin \left( \frac{m\pi y}{l_y} \right)$  and integrated over the length  $l_y$  yielding

$$\left( -\frac{i}{\omega} \left[ D' \left( \left( k_x^2 + (m\pi/l_y)^2 \right)^2 - k_B^4 \right) \right] \right) v_m = A_m \quad (4.23)$$

and substituting  $A_m$  from Eq. (4.20) into Eq. (4.23) after some simplifications, it is found that

$$v_m = \frac{4}{l_y} \frac{p_i a_m(k_y)}{\left[ \left( -\frac{i}{\omega} \left[ D' \left( \left( k_x^2 + (m\pi/l_y)^2 \right)^2 - k_B^4 \right) \right] \right) + \frac{2}{l_y \pi} \left( \int_{-\infty}^{\infty} |a_m(\gamma)|^2 \left( \frac{\omega \rho_0}{k_z} \right) d\gamma \right) \right]} \quad (4.24)$$

where  $k_z = \sqrt{k^2 - \kappa^2 - \gamma^2}$ . In the above simplification, the inter-modal coupling between the pressure modes and the transverse velocity of the plate strip modes in Eq. (4.20) is neglected in the derivation indicated by the term  $|a_m(\gamma)|^2$  in Eq. (4.24).

## 4.2 Transmission coefficient

The transmission coefficient  $\tau$  is defined as the ratio of the transmitted sound power  $W_{tran}$  to the incident sound power  $W_{inc}$ . The sound power transmitted through the plate strip is equal to the sound power radiated into the region  $z > 0$ , hereafter denoted by  $W_{rad2}$ . For clarity and consistency in defining the radiated power of the plate strip, an arbitrary length of plate strip  $L_x$  is retained in the following derivation. Thus, the radiated sound power of the plate strip  $W_{rad2}$  per unit length in the  $x$ -direction is given by

$$W_{rad2} = \frac{1}{2} \operatorname{Re} \left\{ \frac{1}{L_x} \int_{-\infty}^{\infty} \int_0^{L_x} p(x, y) v^*(x, y) dx dy \right\} \quad (4.25)$$

in which the range of the integration 0 to  $l_y$  has been extended to  $\pm\infty$  because the form of  $\tilde{V}_y(\gamma)$  ensures that  $v_y$  is zero outside  $0 < y < l_y$ . Substituting Eq. (4.15) and Eq. (4.18) into Eq. (4.25) for the radiated sound power per unit length, this yields

$$\begin{aligned} W_{rad2} &= \frac{1}{2} \operatorname{Re} \left\{ \frac{1}{L_x} \int_{-\infty}^{\infty} \int_0^{L_x} \frac{1}{2\pi} \int_{-\infty}^{\infty} \frac{\rho_0 ck}{\sqrt{k^2 - k_x^2 - \gamma^2}} \tilde{V}_y(\gamma) e^{-i\gamma y} e^{-ik_x x} d\gamma \right. \\ &\quad \left. \times \frac{1}{2\pi} \int_{-\infty}^{\infty} \tilde{V}_y^*(\gamma') e^{i\gamma' y} e^{ik_x x} d\gamma' dx dy \right\} \\ &= \frac{1}{8\pi^2} \operatorname{Re} \left\{ \int_{-\infty}^{\infty} \frac{\rho_0 ck}{\sqrt{k^2 - k_x^2 - \gamma^2}} |\tilde{V}_y(\gamma)|^2 \left( \int_{-\infty}^{\infty} e^{-i(\gamma - \gamma') y} dy \right) d\gamma \right\} \\ &= \frac{1}{4\pi} \operatorname{Re} \left\{ \int_{-\infty}^{\infty} \frac{\rho_0 ck}{\sqrt{k^2 - k_x^2 - \gamma^2}} |v_m|^2 \left[ \frac{2\pi m / l_y}{\gamma^2 - (m\pi / l_y)^2} \right] \sin \left( \frac{\gamma l_y - m\pi}{2} \right) \right]^2 d\gamma \right\} \end{aligned} \quad (4.26)$$

Hence the total radiated sound power with the necessary condition  $k_x^2 + \gamma^2 \leq k^2$  is

$$W_{rad2} = \frac{1}{4\pi} \sum_{m=1}^{\infty} \left\{ \int_{-\sqrt{k^2-k_x^2}}^{\sqrt{k^2-k_x^2}} \frac{\rho_0 c k}{\sqrt{k^2-k_x^2-\gamma^2}} |v_m|^2 \left[ \frac{2\pi m/l_y}{\gamma^2-(m\pi/l_y)^2} \right] \sin\left(\frac{\gamma l_y - m\pi}{2}\right) \right\}^2 d\gamma \quad (4.27)$$

The incident power per unit length for the plate strip can be expressed as follows

$$W_{inc} = \frac{1}{2} \frac{|p_i|^2 \cos \theta}{\rho_0 c} l_y \quad (4.28)$$

The transmission coefficient is given by

$$\tau = \frac{W_{rad2}}{W_{inc}} \quad (4.29)$$

Substituting Eq. (4.27) and (4.28) into Eq. (4.29) gives

$$\tau = \frac{(\rho_0 c)^2}{2\pi |p_i|^2 \cos \theta} \left\{ \sum_{m=1}^{\infty} \int_{-\sqrt{k^2-k_x^2}}^{\sqrt{k^2-k_x^2}} \frac{k}{\sqrt{k^2-k_x^2-\gamma^2}} |v_m|^2 \left[ \frac{2\pi m/l_y}{\gamma^2-(m\pi/l_y)^2} \right] \sin\left(\frac{\gamma l_y - m\pi}{2}\right) \right\}^2 d\gamma \quad (4.30)$$

The sound transmission loss  $R$  is found from

$$R = 10 \log_{10} \left( \frac{1}{\tau} \right) \quad \text{dB} \quad (4.31)$$

The model was used to evaluate the effect of changing the incident angle, thickness and structural loss factor with a total number of modes  $M = 150$  taken into account in calculation. In the present case, the number of the modes is increased from that considered in section 2 as the frequency range is extended to 10 kHz where 25 waves have cut-on.

Figure 4.5 presents a comparison of the predicted transmission loss calculated using the transmission coefficient in Eq. (4.30) and the transmission coefficient of an infinite plate for a normal incidence which is calculated using Eq. 5.14 of [1]

$$\tau = \frac{4}{\left[ (\omega \rho h - s/\omega) / \rho_0 c \right]^2 + (\omega_0 \rho h \eta / \rho_0 c + 2)^2} \quad (4.32)$$

where  $s$  is the stiffness per unit area and  $\omega_0 = \sqrt{s/(\rho h)}$ .

In general, at frequencies above 100 Hz, the STL of the plate strip tends to the infinite plate result which typically follows the mass-law behaviour. Hence, for this region the STL of the plate strip is mass-controlled. Some dips or ripples in the curve are related to cut-on frequencies and the corresponding modal behaviour while such features are not present in the infinite plate model. At low frequency, or  $\omega \ll \omega_1$ , a stiffness-controlled behaviour appears where a slope of -30 dB/decade occurs rather than -20 dB/decade as indicated by the infinite plate model. At the first cut-on frequency  $\omega_1$ , the transmission loss has a negative value rather than zero as the lowest value which appears in the infinite plate model. This happens as a consequence of the normalization area introduced in the transmission coefficient. Hence the ratio of radiated sound power and incident power can be greater than unity for the case of the plate strip which has a finite dimension in one direction. A more detailed discussion on this issue is given in [13].

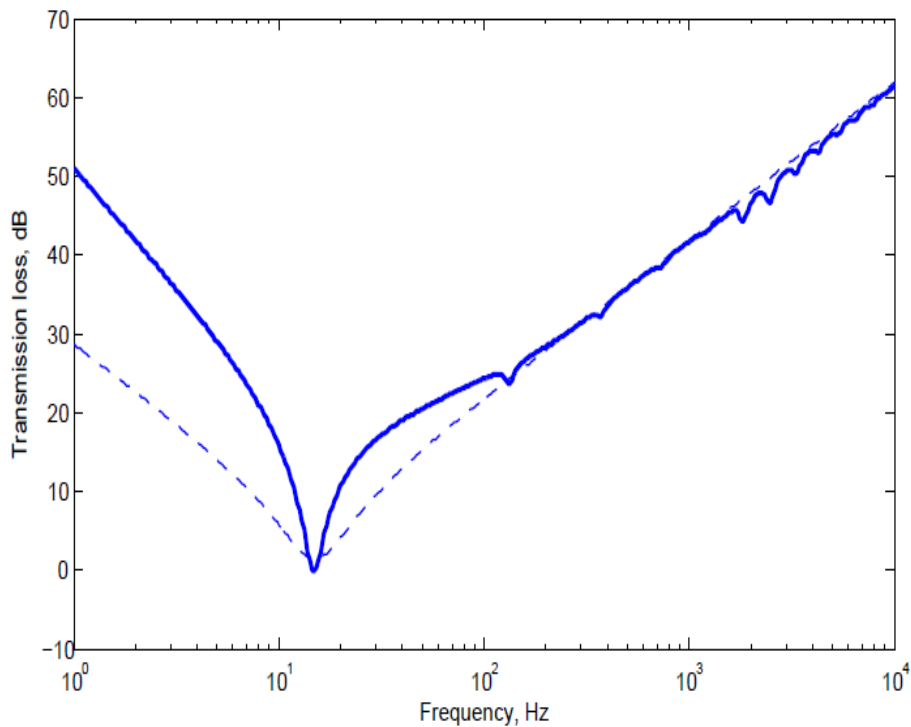


Figure 4.3. STL comparison of the plate strip and the infinite plate for normal incident case (— plate strip; --- infinite plate)

The slope of -30 dB/decade in the stiffness-controlled region can be demonstrated by considering  $\omega \ll \omega_1$  in Eq. (4.24). Hence  $v_m$  reduces to

$$|v_m| = \frac{4}{l_y} \frac{p_i |a_m(k_y)| \omega}{D \left( k_x^2 + (m\pi/l_y)^2 \right)^2 \sqrt{\eta^2 + 1}} \quad (4.33)$$

In this frequency range  $k_x^2 \ll (m\pi/l_y)^2$  so that the transmission coefficient in Eq. (4.30) is finally proportional to the cube of frequency or  $\tau \propto \omega^3$  which results in a slope of -30 dB/decade. If  $\omega \gg \omega_1$ , where the mass-controlled region is found,  $v_m$  in Eq. (4.24) becomes

$$|v_m| = \frac{4}{l_y} \frac{p_i |a_m(k_y)|}{\rho_0 h \omega} \quad (4.34)$$

Accordingly, the transmission coefficient in Eq. (4.30) now is inversely proportional to frequency or  $\tau \propto \omega^{-1}$ . This indicates that a slope of 10 dB/decade applies in this frequency range. However, above the subsequent cut-on frequencies it is found that  $|a_m(k_y)a_m(\gamma)|$  in  $|\tilde{V}_y(\gamma)|$  is proportional to  $1/\sqrt{\omega}$  or  $|a_m(k_y)a_m(\gamma)| \approx 1/\sqrt{\omega}$  hence causing  $\tau \propto \omega^{-2}$ . Thus, the slope of the STL curve increases to 20 dB/decade at high frequency. It should be noted that the transition from 10 dB/decade to 20 dB/decade depends on the incident angle and the width of the plate strip as both variables are contained in the  $a_m$  term. For example for normal incidence case, it is found that the transition occurs at about 340 Hz for 0.5 m width, 170 Hz for 1 m width and 85 Hz for 2 m width. Hence, comparing this with the acoustic wavelength it can be identified as  $\lambda \approx 2l_y$ . A comparison of the STL curve and these slopes is given in Figure 4.4.

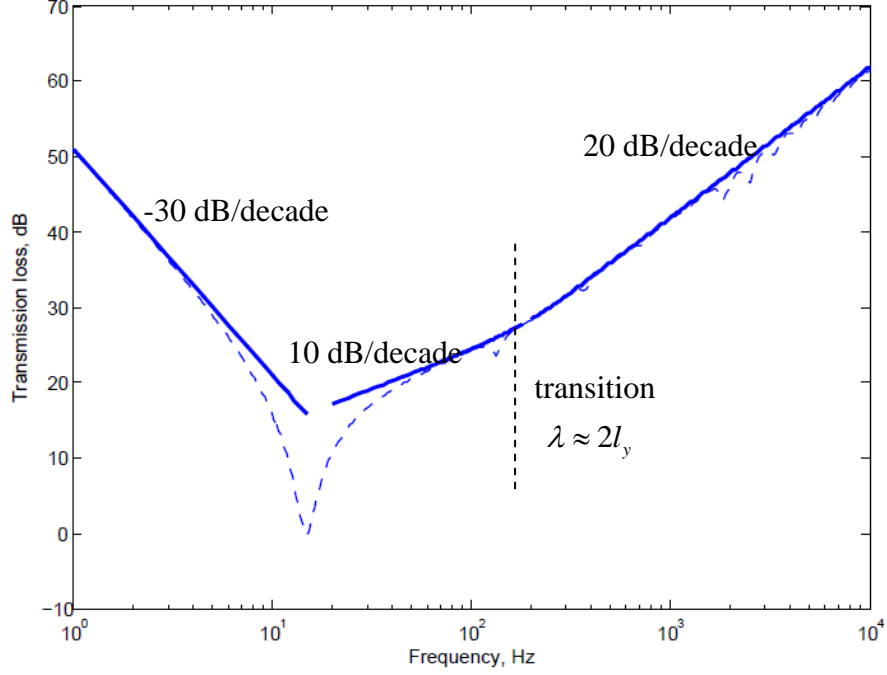


Figure 4.4. STL slope of the stiffness-controlled region and the mass-controlled region.

Figure 4.5 shows results for different angles of incidence. The coincidence frequency depends on the incident angle, with a higher angle corresponding to a lower coincidence frequency. These results have a similar tendency as those obtained by the infinite plate model where the transmission coefficient is calculated using Eq. 7.74 of [2]

$$\tau = \left| \frac{1}{1 + j\omega\rho h \cos\theta \left(1 - (k \sin\theta/k_b)^4\right) / 2\rho_0 c} \right|^2 \quad (4.35)$$

However, in the area close to the coincidence frequency the STL of the infinite plate tends to be higher than that of the plate strip. This difference is affected by the presence of edge mode radiation and cut-on frequencies in the plate strip response. However, when the incident wave is almost parallel to the structure with increasing incident angle, for frequencies below the coincidence frequency it can be seen that the STL of the infinite plate is lower than that obtained by the plate strip model. This is caused by the radiation ratio of the infinite plate which is given by  $\sigma_{\text{inf}} = 1/\cos\theta$ . Therefore, it increases when the incident angle increases and becomes infinite when

$\theta = 90^\circ$  while that of a finite structure remains finite [14]. Meanwhile, above the coincidence frequency, the results of both models are in good agreement.

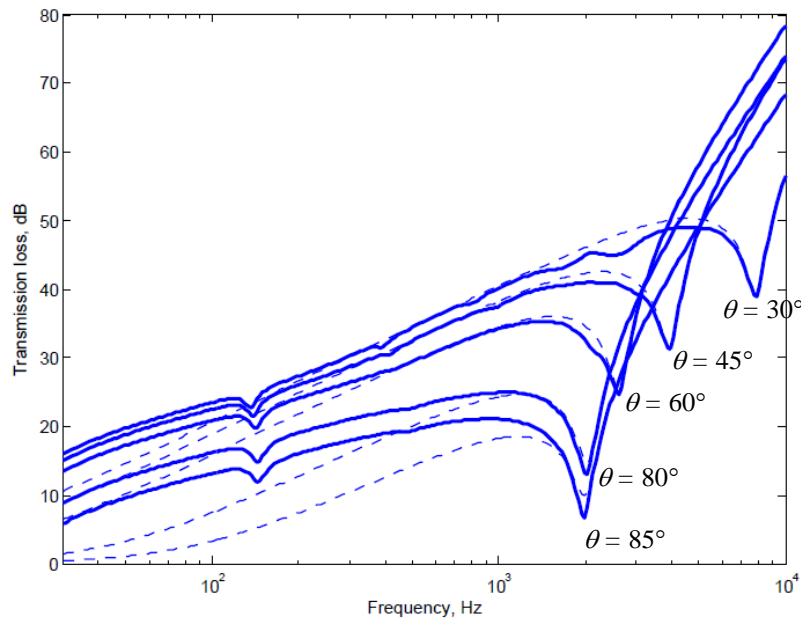
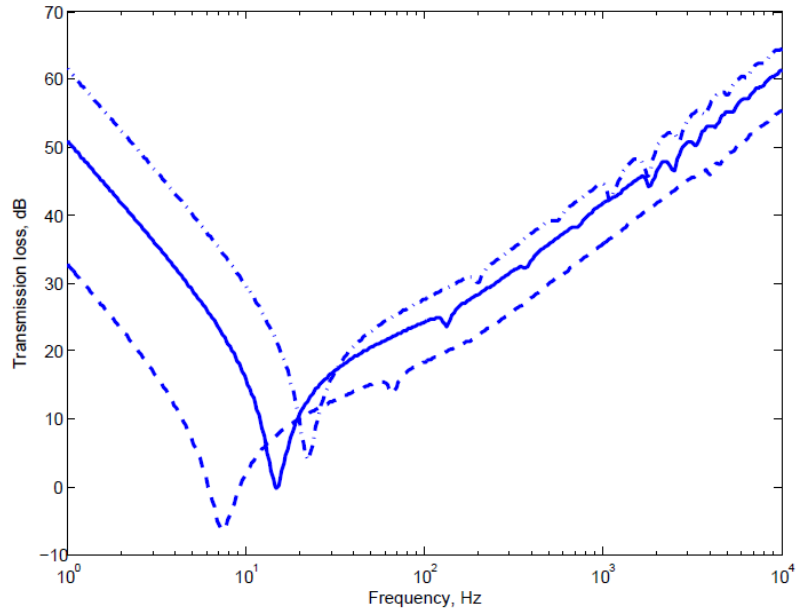
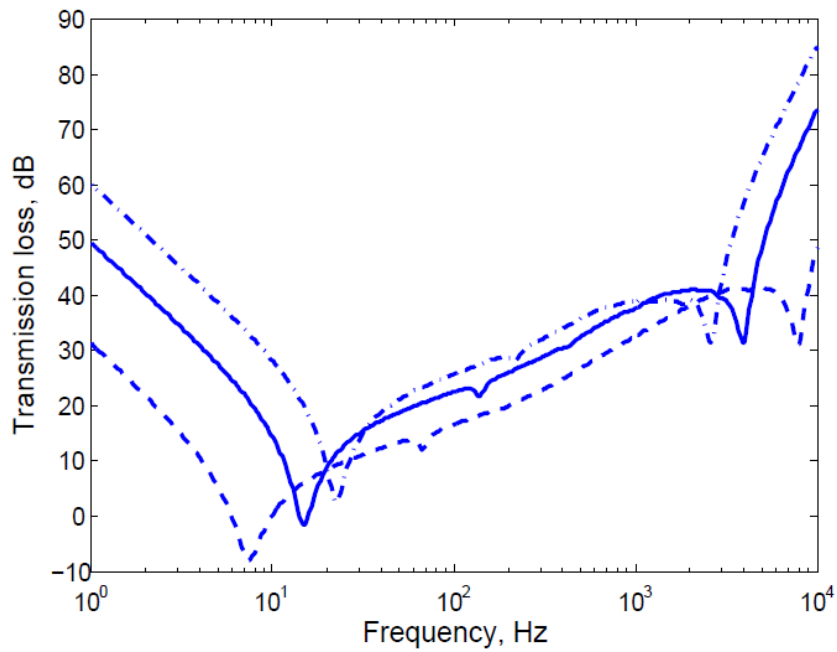


Figure 4.5. STL comparison of the plate strip and the infinite plate for obliquely incident case (— plate strip; --- infinite plate).

Results for different thicknesses for normal incidence are shown in Figure 4.6(a). Here the analytical model again behaves as expected with the first panel resonance (cut-on frequency) becoming lower and the STL values reducing when the thickness reduces. The same situation also appears when the plate strip is obliquely excited as can be seen from Figure 4.6(b). However, the corresponding coincidence frequency now also exists and it shifts to a lower frequency with increasing thickness.



(a)

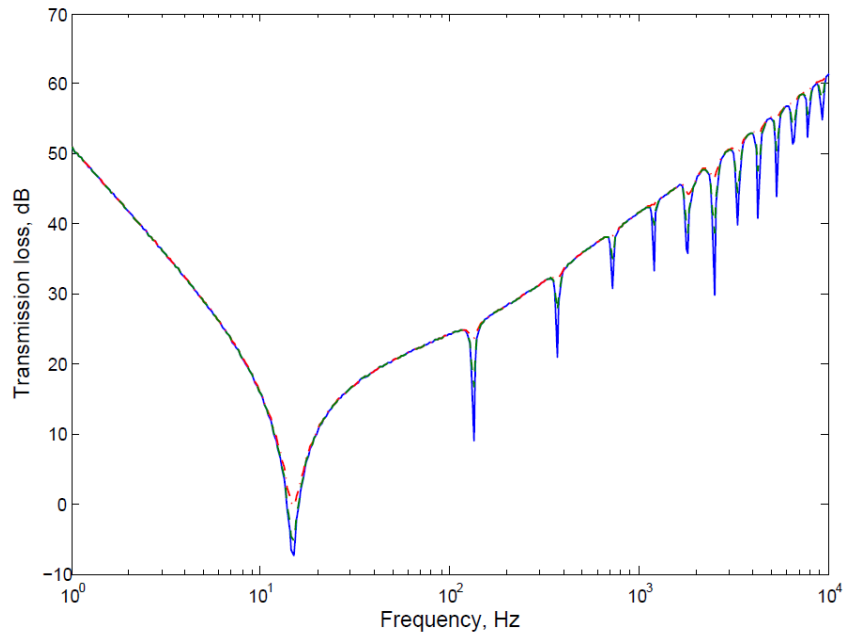


(b)

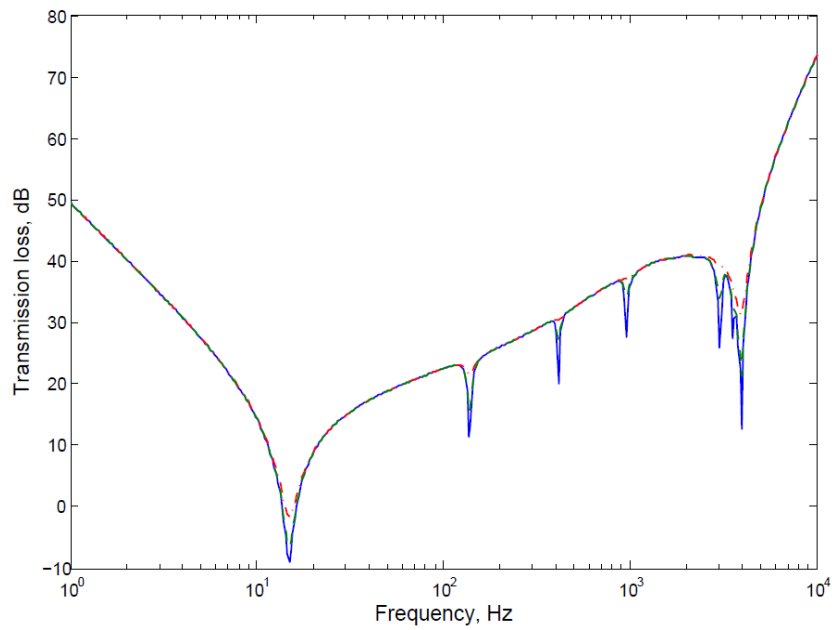
Figure 4.6. Effect of changing thickness of the plate strip on the sound transmission loss: (a) normal incidence; (b) oblique incidence (---  $h = 3$  mm ; —  $h = 6$  mm ; - · - ·  $h = 9$  mm).

Figure 4.7(a) presents the effect of the structural damping loss factor on the sound transmission loss values for normal incidence. It is clear that this factor has a

large influence at the cut-on frequencies but negligible effect elsewhere. The same tendency is also found for oblique incidence as shown in Figure 4.7(b).



(a)



(b)

Figure 4.7. Effect of structural loss factor of the plate strip on the sound transmission loss: (a) normal incidence ; (b) oblique incidence at angle  $45^\circ$  ( —  $\eta = 0.01$  ; - -  $\eta = 0.03$ , - · -  $\eta = 0.1$ )

### 4.3 Diffuse sound field

The diffuse sound field excitation is formulated as the superposition of uncorrelated plane waves with equal amplitude in all direction. The sound transmission is then obtained by integrating the response of all incident plane waves over the incident angle and weighting them with the solid angle to account for the directional distribution. Therefore, the sound transmission loss for a diffuse field excitation is expressed as

$$\tau_d = \frac{\int_0^{2\pi} \int_0^{\theta_{\text{lim}}} \tau(\theta, \varphi) \sin \theta \cos \theta d\theta d\varphi}{\int_0^{2\pi} \int_0^{\theta_{\text{lim}}} \sin \theta \cos \theta d\theta d\varphi} = \frac{1}{\pi} \int_0^{2\pi} \int_0^{\theta_{\text{lim}}} \tau(\theta, \varphi) \sin \theta \cos \theta d\theta d\varphi \quad (4.36)$$

where  $\theta_{\text{lim}}$  is the upper elevation angle which is typically taken equal to  $78^\circ$  for field incidence case and which is  $90^\circ$  for the full random incidence case [10]. Historically, the upper elevation angle, i.e. the field incidence case, was motivated to provide a better fit to measurement results so this is actually an empirical approach. However, some physical explanations of this which justify it as acceptable are available by realizing that the incident energy at grazing incidence is difficult to produce in real situations [15, 16].

Figure 4.8 presents a comparison of the sound transmission loss between the plate strip and the infinite plate for the diffuse field case. The plate strip and the infinite plate are calculated under the random incidence excitation ( $0^\circ \leq \theta \leq 90^\circ$ ) and the field incidence one ( $0^\circ \leq \theta \leq 78^\circ$ ). It is clear that the dip at around 2 kHz is associated with the critical frequency. Above this frequency, the plate strip and the infinite plate produce a similar curve. However, below this frequency the STL of the plate strip is higher by 6.5 dB at low frequency than that of the infinite plate. This difference reduces with increasing frequency; for example 2.7 dB difference is found at around the critical frequency. This difference comes about because a finite extent in one dimension of the plate strip introduces a spatial windowing effect on the infinite baffle [14]. Accordingly, the radiation ratio of the infinite plate is modified to remain finite for increasing incident angle rather than becoming infinite. This leads to a higher STL for the plate strip. This situation is also illustrated in Figure 4.5 in section 4.2 for oblique incidence. The relation of the incident angle with various

Helmholtz numbers was presented in [14] for the case of a finite plate. When the plate strip is calculated using the field incidence method, below the critical frequency, its STL is getting closer to that obtained for the infinite plate particularly at high frequencies. Above the critical frequency, a similar curve is seen for both models.

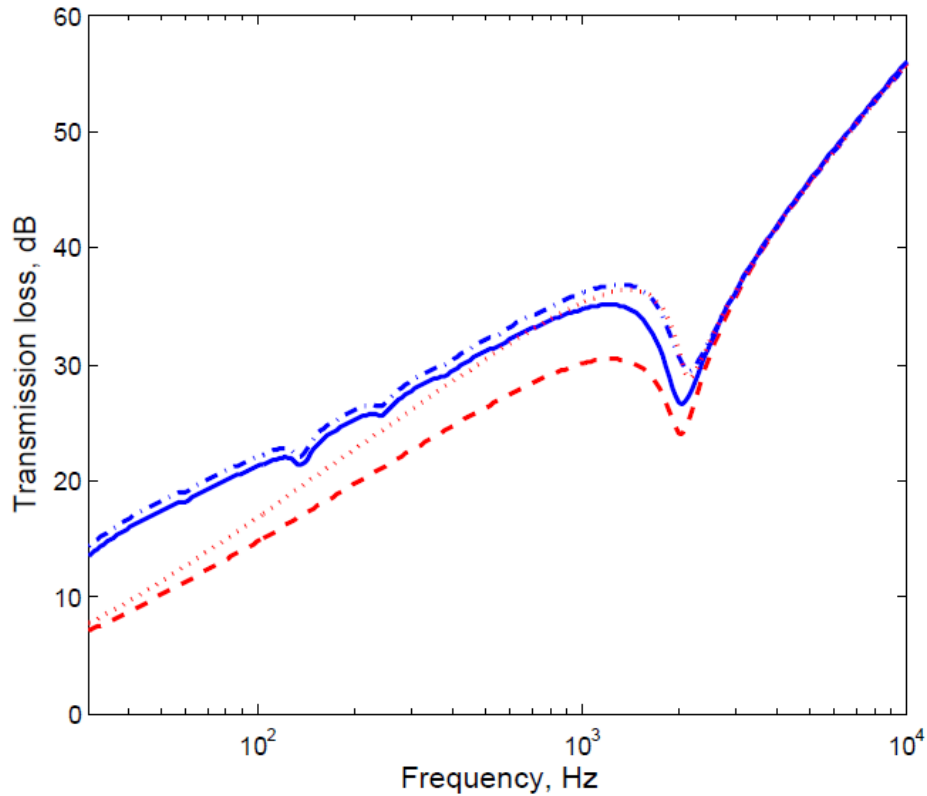


Figure 4.8. STL of plate strip under a diffuse sound field excitation: random incidence ( $0^\circ \leq \theta \leq 90^\circ$ ): (— Plate strip; --- infinite plate); field incidence ( $0^\circ \leq \theta \leq 78^\circ$ ): (· - · Plate strip; ··· infinite plate).

#### 4.4 Summary

An analytical solution for sound transmission through a plate strip has been derived by considering acoustic plane wave excitation, internal and acoustic damping but neglecting the cross-term contributions. Comparing the results with that of the infinite plate, some differences occur. For the normal incidence case, it is found that at high frequency, the STL of the plate strip converges to that of the infinite plate while at low frequency a slope of -30 dB/decade is found rather than

the -20 dB/decade that is normally found in the STL of an infinite plate. Dips are found corresponding to the cut-on frequencies.

For the oblique incidence case, the analytical model behaves as expected considering the coincidence frequencies when the incidence angle is varied. These match with the infinite plate results. However, well below the coincidence frequency the STL of the plate strip is greater than that of the infinite plate due to its finite width.

The internal damping loss factor effectively determines the STL values around the cut-on frequencies and the coincidence frequencies. Elsewhere, the damping has a negligible effect. Meanwhile, varying the thickness will shift the first cut-on frequency and coincidence frequency while the STL values increase as the thickness increases.

Under random incidence, the plate strip model produces the same results as an infinite plate above the critical frequency. Below this frequency, the STL values of the plate strip are higher than those obtained using the infinite plate model. Closer results are found around the critical frequency and just below this frequency when both the plate strip and the infinite plate are excited by the field incidence limited to  $78^\circ$ .

## 5. Conclusions

A study of the vibro-acoustic behaviour of a plate strip has been presented. An analytical model has been developed in order to investigate the plate strip in terms of its mobility, its sound power radiation and its sound transmission loss. Some concluding remarks can be made as follows:

1. The mobility of the plate strip due to a point force excitation is stiffness-controlled at low frequency while it tends to be similar to that of an infinite plate at high frequencies. Peaks occur at the cut-on frequencies with magnitudes that depend on the location of the excitation point. Damping has an effect only around the cut-on frequencies.
2. It is clear that the plate strip still radiates sound below the critical frequency even if it is less than above the critical frequency. This sound is produced by nearfield waves in the vicinity of the forcing point and by ‘edge modes’, that is waves with an axial wavenumber smaller than the acoustic wavenumber while the transverse wavenumber is greater than the acoustic wavenumber. Therefore, it is clear that the finite width and the point force excitation influence the sound power radiation below the critical frequency.
3. The sound transmission loss of the plate strip for normal incidence converges to the mass-law result at high frequencies. At low frequency, below the first cut-on frequency, a stiffness-controlled region appears, while the mass-controlled region exists above the first cut-on frequency. The slope at low frequencies is modified from the result for an infinite plate when the width is less than half the acoustic wavelength. Some dips or ripples in the curve are related to various cut-on frequencies. Such features are not present in an infinite model.

The results presented here can be used as benchmark solutions for validating numerical methods such as waveguide FE/BE.

## References

1. Fahy, F. and P. Gardonio, *Sound and Structural Vibration: Radiation, Transmission and Response*. 2nd ed. 2006, London: Academic Press.
2. Cremer, L., M. Heckel, and B.A.T. Petterson, *Structure-Borne Sound*. 3rd edition ed. 2005, Berlin: Springer.
3. Gardonio, P. and M.J. Brennan, *Mobility and Impedance Method in Structural Dynamics*. chapter 9 in *Advanced Applications in Acoustics, Noise and Vibration*, ed. F.J. Fahy and J.G. Walker. 2004: Spon Press.
4. Cremer, L., M. Heckl, and E.E. Ungar, *Structure-borne Sound (second ed.)*. 1988, Berlin: Springer.
5. Williams, E., *Fourier Acoustics: Sound Radiation and Nearfield Acoustical Holography*. 1999: Academic Press.
6. Junger, M.C. and D. Feit, *Sound, structures, and their interaction* 1972, Cambridge, Mass.: MIT Press.
7. Sakagami, K., et al., *Sound radiation from a baffled elastic plate strip of infinite length with various concentrated excitation forces*. *Applied Acoustics*, 1998. **55**(3): p. 181-202.
8. Maidanik, G., *Response of Ribbed Panels to Reverberant Acoustic Fields*. *J. Acoust. Soc. Am.*, 1962. **34**(6): p. 809.
9. Wallace, C., *Radiation Resistance of a Rectangular Panel*. *J. Acoust. Soc. Am.*, 1972. **51**(3B): p. 946.
10. Beranek, L.L., *Noise and Vibration Control* 1971, New York: McGraw-Hill
11. Li, W.L. and H.J. Gibelung, *Determination of the mutual radiation resistance of a rectangular plate and their impact on the radiated sound power*. *Journal of Sound and Vibration*, 2000. **229**(5): p. 1213-1233.
12. London, A., *Transmission of reverberant sound through single walls*. *Research Nat. Bur. of standard*, 1949. **42**(605).
13. Thompson, D.J., P. Gardonio, and J. Rohlfing, *Can a transmission coefficient be greater than unity?* *Applied Acoustics*, 2009. **70**(5): p. 681-688.
14. Villot, M., C. Guigou, and L. Gagliardini, *Predicting the acoustical radiation of finite size multi-layered structures by applying spatial windowing of infinite structures*. *Journal of Sound and Vibration*, 2001. **245**(3): p. 433-455.

15. Mulholland, K.A., H.D. Parbrook, and A. Cummings, *The transmission loss of double panels*. Journal of Sound and Vibration, 1967. **6**(3): p. 324-334.
16. Leppington, F.G., et al., *Resonant and non-resonant acoustic properties of elastic panels. II. The transmission problem*. Proceedings of the Royal Society of London. Series A, Mathematical and Physical Sciences, 1987. **412**(1843): p. 309-337.

## Appendix A Out-of plane displacement of a plate strip due to a point force

The out-of plane displacement of the infinite plate strip vibrating in order  $m$  contained in Eq. (2.2) can be written as

$$\begin{aligned} w_m(x \leq 0) &= A_{1,m} e^{ik_{x1,m}x} + A_{2,m} e^{ik_{x2,m}x} \\ w_m(x \geq 0) &= A_{3,m} e^{-ik_{x1,m}x} + A_{4,m} e^{-ik_{x2,m}x} \end{aligned} \quad (\text{A.1})$$

where  $k_{x1,m}$  and  $k_{x2,m}$  are given in Eq. (2.6).

The generalized force acting on the  $m^{\text{th}}$  order motion is given by

$$F_m = F \sin\left(\frac{m\pi y_0}{l_y}\right) \quad (x=0) \quad (\text{A.2})$$

The boundary conditions for such structures evaluated at  $x=0$  are as follows

1. Continuity equation ; equal displacement

$$\begin{aligned} w_m(0)_- &= w_m(0)_+ \\ \left. \begin{aligned} w_m(0, y)_- &= (A_{1,m} + A_{2,m}) \\ w_m(0, y)_+ &= (A_{3,m} + A_{4,m}) \end{aligned} \right\} A_{1,m} + A_{2,m} = A_{3,m} + A_{4,m} \end{aligned} \quad (\text{A.3})$$

2. Continuity of rotation

$$\left. \frac{\partial w_m(x)_-}{\partial x} = \frac{\partial w_m(x)_+}{\partial x} \right|_{x=0} \rightarrow A_{1,m}(ik_{x1,m}) + A_{2,m}(ik_{x2,m}) = -iA_{3,m}k_{x1,m} - iA_{4,m}k_{x2,m} \quad (\text{A.4})$$

3. Continuity of bending moment

$$\left. \frac{\partial^2 w_m(x)_-}{\partial x^2} = \frac{\partial^2 w_m(x)_+}{\partial x^2} \right|_{x=0} \rightarrow -A_{1,m}k_{x1,m}^2 - A_{2,m}k_{x2,m}^2 = -A_{3,m}k_{x1,m}^2 - A_{4,m}k_{x2,m}^2 \quad (\text{A.5})$$

#### 4. Force equilibrium condition

$$S_m(0, y)_+ - S_m(0, y)_- = F_m \quad (\text{A.6})$$

$$\left( [A_{3,m}(ik_{x1,m}^3) + A_{4,m}(ik_{x2,m}^3)] - \left[ (2-\nu) [A_{3,m}(-ik_{x1,m}) + A_{4,m}(-ik_{x2,m})] \left( \frac{m\pi}{l} \right)^2 \right] \right) - \left( [A_{1,m}(-ik_{x1,m}^3) + A_{2,m}(-ik_{x2,m}^3)] - \left[ (2-\nu) [A_{1,m}(ik_{x1,m}) + A_{2,m}(ik_{x2,m})] \left( \frac{m\pi}{l} \right)^2 \right] \right) = \frac{F_m}{D'}$$

Using the relation from (A.4)

$$-A_{3,m}k_{x1,m}^3 - A_{4,m}k_{x2,m}^3 - A_{1,m}k_{x1,m}^3 - A_{2,m}k_{x2,m}^3 = \frac{F_m}{D'} \quad (\text{A.7})$$

From Eq. (A.3) and Eq. (A.5) the following relations are obtained

$$\begin{aligned} A_{1,m} &= A_{3,m} \quad ; \quad A_{2,m} = A_{4,m} \\ A_{4,m} &= -\frac{k_{x1,m}}{k_{x2,m}} A_{3,m} \end{aligned} \quad (\text{A.8})$$

By substituting Eq. (A.8) into Eq. (A.7) this yields

$$\begin{aligned} iA_{3,m} \left( k_{x1,m}^3 - k_{x2,m}^3 \frac{k_{x1,m}}{k_{x2,m}} + k_{x1,m}^3 - k_{x2,m}^3 \frac{k_{x1,m}}{k_{x2,m}} \right) &= \frac{F_m}{D'} \\ A_{3,m} &= \frac{-iF_m}{2D'k_{x1,m}(k_{x1,m}^2 - k_{x2,m}^2)} \end{aligned}$$

The other coefficients will be

$$\begin{aligned} A_{1,m} &= \frac{-iF_m}{2D'k_{x1,m}(k_{x1,m}^2 - k_{x2,m}^2)} \\ A_{2,m} &= \left( -\frac{k_{x1,m}}{k_{x2,m}} \right) \frac{-iF_m}{2D'k_{x1,m}(k_{x1,m}^2 - k_{x2,m}^2)} \\ A_{4,m} &= \left( -\frac{k_{x1,m}}{k_{x2,m}} \right) \frac{-iF_m}{2D'k_{x1,m}(k_{x1,m}^2 - k_{x2,m}^2)} \end{aligned}$$

Based on these coefficients, the solution may be written as follows

$$\begin{aligned}
w_m(x \leq 0) &= \frac{-iF_m}{2D'k_{x1,m}(k_{x1,m}^2 - k_{x2,m}^2)} \left[ e^{ik_{x1,m}x} - \frac{k_{x1,m}}{k_{x2,m}} e^{ik_{x2,m}x} \right] \\
w_m(x \geq 0) &= \frac{-iF_m}{2D'k_{x1,m}(k_{x1,m}^2 - k_{x2,m}^2)} \left[ e^{-ik_{x1,m}x} - \frac{k_{x1,m}}{k_{x2,m}} e^{-ik_{x2,m}x} \right]
\end{aligned} \tag{A.9 a,b}$$

The complete solution is given by

$$\begin{aligned}
w(x \leq 0, y) &= \sum_{m=1}^{\infty} \frac{-iF_m}{2D'k_{x1,m}(k_{x1,m}^2 - k_{x2,m}^2)} \left[ e^{ik_{x1,m}x} - \frac{k_{x1,m}}{k_{x2,m}} e^{ik_{x2,m}x} \right] \sin\left(\frac{m\pi y}{l_y}\right) \\
w(x \geq 0, y) &= \sum_{m=1}^{\infty} \frac{-iF_m}{2D'k_{x1,m}(k_{x1,m}^2 - k_{x2,m}^2)} \left[ e^{-ik_{x1,m}x} - \frac{k_{x1,m}}{k_{x2,m}} e^{-ik_{x2,m}x} \right] \sin\left(\frac{m\pi y}{l_y}\right)
\end{aligned} \tag{A.10 a,b}$$

## Appendix B Modulus squared of plate velocity in wavenumber domain

The plate velocity in the wavenumber domain for a single mode  $m$  is given by Eq. (2.19) as follows

$$\begin{aligned} \tilde{V}(k_x, k_y) = & \frac{\omega F_m}{2D'k_{x1,m}(k_{x1,m}^2 - k_{x2,m}^2)} \left[ \int_{-\infty}^0 \left( e^{i(k_{x1,m} + k_x)x} - \frac{k_{x1,m}}{k_{x2,m}} e^{i(k_{x2,m} + k_x)x} \right) dx \right. \\ & \left. + \left( \int_0^{\infty} e^{-i(k_{x1,m} - k_x)x} - \frac{k_{x1,m}}{k_{x2,m}} e^{-i(k_{x2,m} - k_x)x} \right) dx \right] \left[ \int_0^{l_y} \left( \frac{e^{i(m\pi/l_y + k_y)y} - e^{-i(m\pi/l_y - k_y)y}}{2i} \right) dy \right] \end{aligned} \quad (\text{B.1})$$

From Eq. (B.1), the plate velocity in the wavenumber domain in the  $x$ -direction is

$$\begin{aligned} \tilde{V}_x(k_x) = & \frac{\omega F_n}{2D'k_{x1}(k_{x1}^2 - k_{x2}^2)} \left( \left[ \frac{1}{i(k_{x1} + k_x)} - \frac{k_{x1}}{k_{x2}} \frac{1}{i(k_{x2} + k_x)} \right] \right. \\ & \left. + \left[ \frac{1}{i(k_{x1} - k_x)} - \frac{k_{x1}}{k_{x2}} \frac{1}{i(k_{x2} - k_x)} \right] \right) \\ = & \frac{\omega F_n}{2D'k_{x1}(k_{x1}^2 - k_{x2}^2)} \left( -\frac{2ik_{x1}}{(k_{x1}^2 - k_x^2)} + \frac{2ik_{x1}}{k_{x2}} \left( \frac{k_{x2}}{k_{x2}^2 - k_x^2} \right) \right) \quad (\text{B.2}) \\ = & \frac{i\omega F_n}{D'(k_{x1}^2 - k_{x2}^2)} \left( \frac{1}{(k_{x2}^2 - k_x^2)} - \frac{1}{(k_{x1}^2 - k_x^2)} \right) \\ = & \frac{i\omega F_n}{D'(k_{x1}^2 - k_x^2)(k_{x2}^2 - k_x^2)} \end{aligned}$$

while that of the  $y$  dependent plate velocity in the wavenumber domain is

$$\tilde{V}_y(k_y) = \left( \frac{m\pi/l_y}{k_y^2 - (m\pi/l_y)^2} \right) [(-1)^m e^{ik_y l_y} - 1] \quad (\text{B.3})$$

The absolute value of Eq. (B.3) is

$$\begin{aligned}
|\tilde{V}_y(k_y)| &= \left| \frac{m\pi/l_y}{k_y^2 - (m\pi/l_y)^2} \right| \left| e^{i(k_y l_y - m\pi)} - 1 \right| \\
&= \left| \frac{m\pi/l_y}{k_y^2 - (m\pi/l_y)^2} \right| \left| \cos(k_y l_y - m\pi) + i \sin(k_y l_y - m\pi) - 1 \right| \\
&= \left| \frac{m\pi/l_y}{k_y^2 - (m\pi/l_y)^2} \right| \sqrt{2(1 - \cos(k_y l_y - m\pi))} \\
&= \left| \frac{m\pi/l_y}{k_y^2 - (m\pi/l_y)^2} \right| \sqrt{4 \sin^2 \left( \frac{k_y l_y - m\pi}{2} \right)}
\end{aligned} \tag{B.4}$$

The plate velocity in  $x$  and  $y$  directions may be written as

$$\tilde{V}(k_x, k_y) = \tilde{V}_x(k_x) \tilde{V}_y(k_y) \tag{B.5}$$

Hence the modulus of  $\tilde{V}(k_x, k_y)$  can be written as combination of Eq. (B.2) and (B.4) as

$$|\tilde{V}(k_x, k_y)| = \left| \frac{\omega F_n}{D'(k_{x1}^2 - k_x^2)(k_{x2}^2 - k_x^2)} \right| \left| \frac{m\pi/l_y}{k_y^2 - (m\pi/l_y)^2} \right| \sqrt{4 \sin^2 \left( \frac{k_y l_y - m\pi}{2} \right)} \tag{B.5}$$

Thus the modulus squared of  $\tilde{V}(k_x, k_y)$  is

$$|\tilde{V}(k_x, k_y)|^2 = \left| \frac{\omega F_n}{D'(k_{x1}^2 - k_x^2)(k_{x2}^2 - k_x^2)} \right|^2 \left[ \frac{2\pi m/l_y}{k_y^2 - (m\pi/l_y)^2} \right]^2 \sin^2 \left( \frac{k_y l_y - m\pi}{2} \right) \tag{B.6}$$